What drives Alpine Tethys opening: clues from the review of geological data and model predictions

Manuel Roda[a], Alessandro Regorda[a], Maria Iole Spalla[a], Anna Maria Marotta[a]

[a]Universita' degli Studi di Milano, Dipartimento di Scienze della Terra, Via Mangiagalli 34, 20133 - Milano (Italy)

Abstract

Permo-Triassic remnants (300-220 Ma) of high-temperature metamorphism associated with large gabbro bodies occur in the Alps and indicate a high thermal regime compatible with lithospheric thinning. During the Late Triassic-Early Jurassic an extensional tectonics leads to the break-up of Pangea continental lithosphere and the opening of Alpine Tethys Ocean (170-160 Ma), as testified by the ophiolites outcropping in the Central-Western Alps and Apennines. We revise geological data from the Permian to Jurassic of the Alps and Northern Apennines, focusing on continental and oceanic basement rocks, and predictions of existing numerical models of post-collisional extension of continental lithosphere and successive rifting and oceanization. The aim is to test whether the transition from the Permo-Triassic extensional tectonics to the Jurassic opening of Alpine Tethys occurred. We enforce the interpretation that a forced extension of 2 cm/yr of the post-collisional lithosphere results in a thermal state compatible with the Permo-Triassic high-temperature event suggested by pressure and temperature conditions of metamorphic rocks and widespread igneous activity. Extensional or transtensional tectonics is also in agreement with the generalized subsidence indicated by the deposition of sedimentary successions with deepening upward facies occurred in the Alps from the Permian to Jurassic. Furthermore, a rifting developed on a thermally perturbed lithosphere agrees with a hyperextended configuration of the Alpine Tethys rifting and with the duration of the extension necessary to the oceanization. The review supports the interpretation of Alpine Tethys opening developed on a lithosphere characterized by a thermo-mechanical configuration inherited by the post-Variscan extension which affected Pangea during the Permian and Triassic. Therefore, a long-lasting period of active extension can be envisaged for the breaking of Pangea supercontinent, starting from the unrooting of the Variscan belts, followed by the Permo-Triassic thermal high, and ending with the crustal break-up and the formation of the Alpine Tethys Ocean.

Keywords: Alpine Tethys Rifting, Numerical modeling, Permo-Triassic high thermal regime, Variscan collision

1 INTRODUCTION

Continental crustal slices preserving pre-Alpine metamorphic imprints are widely described in the Alps and Apennines. Variscan-age eclogites (430-326 Ma), generated from continental, oceanic and mantle rocks belonging to these slices, suggest a pre-Alpine burial of continental crust in a context of oceanic lithosphere subduction underneath a continental upper plate, followed by continental collision (e.g., Marotta & Spalla, 2007; Spalla et al., 2014; Spalla & Marotta, 2007; von Raumer, Bussy, Schaltegger, Schulz, & Stampfli, 2013). Permo-Triassic records (300-220 Ma) of high-temperature metamorphism mainly occur within Austroalpine and Southalpine domains of the Alps (Figure 1) and are associated with widespread emplacement of large gabbro bodies (Figure 2) and acidic intrusives, together with spinel-plagioclase bearing peridotites. This accounts for an increase in the thermal regime (e.g., Lardeaux & Spalla, 1991; Marotta, Spalla, & Gosso, 2009; Schuster & Stüwe, 2008; Spalla et al., 2014) related to asthenospheric upwelling and lithospheric thinning (e.g., Beardsmore & Cull, 2001; Sandiford & Powell, 1986; Thompson, 1981). Late Triassic-Early Jurassic extensional tectonics leads to the break-up of the Pangea continental lithosphere and the opening of the Alpine Tethys Ocean, testified by the occurrence of ophiolitic sequences in the Alps and Apennines (Figure 3).

The geodynamic significance of the Permo-Triassic high temperature and low pressure metamorphic event has been widely debated. Some authors propose a late-Variscan post-orogenic collapse (e.g., Desmons, Compagnoni, Cortesogno, Frey, & Gaggero, 1999; Gardien, Reusser, & Marquer, 1994; Neubauer, Frisch, Schmerold, & Schlöser, 1989; Picazo et al., 2016), active in a mainly strike-slip dominated tectonics (Arthaud & Matte, 1977; Cassinis & Perotti, 1994; von Raumer et al., 2013). From ca. 260 Ma, a thermal relaxation of the lithosphere would have characterized the entire Triassic until ca. 200-180 Ma, when the Mesozoic continental rifting started (Picazo et al., 2016).

Alternatively, numerical models (Marotta & Spalla, 2007; Marotta et al., 2009; Spalla et al., 2014) support the interpretation of a long-lasting lithospheric thinning and extensional tectonics leading to the Mesozoic continental rifting (e.g., Bertotti, Siletto, & Spalla, 1993; Diella, Spalla, & Tunesi, 1992; Lardeaux & Spalla, 1991). Long-lasting extension process has already been proposed for the opening of the Central Atlantic Ocean (from the Permian to Early Jurassic, Piqué & Laville, 1996) and for the Northern Atlantic region (Doré & Stewart, 2002). In the latter, a sequence of rift basins, from Permian to Cretaceous in age, has been described occurring before the opening of the ocean (e.g., Doré & Stewart, 2002), making the rifting of the North Atlantic Ocean a long-lasting process characterized by successive extensional stages associated with a migration of eulerian poles, as testified by the anti-clockwise and successive clockwise rotation of superposed rift axes (Doré & Stewart, 2002).

In this work, we revise the Permo-Jurassic geological data from the Alps and Northern Apennines (Figures 1, 2, 3) and the predictions of existing models of post-collisional extension of continental lithosphere (Marotta et al., 2009) and of rifting and oceanization (Marotta, Roda, Conte, & Spalla, 2018). The goal is to test whether a protracted extension active on a lithosphere thermally and mechanically perturbed by the Variscan subduction and collision, can lead the Mesozoic rifting and the oceanization of the Alpine Tethys. We quantify the impact of extensional tectonics on the thermal regime of the continental lithosphere of Pangea, and we also calculate the melting fraction of the lithospheric mantle to be compared with the different magmatic suits of continental gabbros and ophiolite

2 TECTONIC EVOLUTION AND METAMORPHIC AND MAGMATIC RECORDS

The Alps and Apennines belts developed during the closure of the Mesozoic Tethys along two opposite subduction zones active during Cretaceous-Oligocene time for the Alpine system and from Eocene time to the present day for the Apennines system (e.g., Carminati & Doglioni, 2012; Dal Piaz, 2010; Handy, Schmid, Bousquet, Kissling, & Bernoulli, 2010). Pre-Alpine metamorphic and magmatic records from the Alps occur within the four main tectonic domains, namely Southalpine, Austroalpine, Penninic and Helvetic. The Southalpine domain consists of a south-verging thrust system that has been active since Cretaceous time, involving Palaeozoic continental basement and Permo-Cenozoic cover units, both locally affected by very low-grade Alpine metamorphism (Brack, 1981; Zanoni & Spalla, 2018; Zanoni, Spalla, & Gosso, 2010, and refs therein). The Penninic domain consists of a mélange of crustal slices deriving from both pre-Alpine continental and Mesozoic oceanic lithosphere, the latter tectonically sampled from the subducted Alpine Tethys Ocean (e.g., Malatesta, Crispini, Federico, Capponi, & Scambelluri, 2012; Malatesta, Gerya, Crispini, Federico, & Capponi, 2013; Platt, 1986; Polino, Dal Piaz, & Gosso, 1990; Roda, Marotta, & Spalla, 2010; Roda, Spalla, & Marotta, 2012; Spalla, Gosso, Marotta, Zucali, & Salvi, 2010; Spalla, Lardeaux, Dal Piaz, Gosso, & Messiga, 1996; Stöckhert & Gerya, 2005). In contrast, ophiolites do not occur in the Austroalpine domain although they are tectonically coupled together with Mesozoic sediments along the external boundary of the domain, under high-pressure (HP) metamorphic conditions (Lardeaux, 2014; Roda et al., 2012; Spalla et al., 1996). Finally, the Helvetic domain consists of an Europe-verging thrust system that includes basement and cover slices stacked during the late stages of the Alpine continental collision since Tertiary (Bousquet et al., 2004; Dal Piaz, 2010; Polino et al., 1990).

Due to the weak Alpine metamorphism and deformation, the Helvetic and Southalpine domains broadly preserve pre-Alpine metamorphic, structural and stratigraphic imprints. Pre-Alpine imprints and igneous relics are also preserved in Penninic and Austroalpine domains, even if pervasive Alpine structural and metamorphic reworking shapes them into small-sized relicts, inhibiting the correlation of pre-Alpine structures over a regional scale.
These records consist of high-temperature low-pressure (HT-LP) metamorphic relicts and Permo-Triassic gabbro bodies, and postdate structures and metamorphic imprints developed during the Variscan convergence.
Variscan metamorphic imprints are widely recorded in the Alpine continental crust (Figure 1) and consist of eclogite, granulite and amphibolite facies rocks (Spalla & Marotta, 2007).

We integrate the geological data of Alpine ophiolites and age data and tectono-magmatic characterization of ophiolites from the Northern Apennines. The Northern Apennines are characterized by oceanic and continental units (Figure 3) that widely escaped subduction-related metamorphism. Oceanic rocks occur in the Internal and External Ligurian units that are deformed under low-pressure and low-temperature metamorphic conditions (Donatio, Marroni, & Rocchi, 2013; Marroni & Pandolfi, 2007). The Internal Ligurian units consist of ophiolites of Jurassic age overlain by a sedimentary sequence of Late Jurassic to Paleocene age, whereas the External Ligurian units comprise Late-Cretaceous sedimentary mélanges including slide-blocks of ophiolites at the base (Marroni, Molli, Ottri, & Pandolfi, 2001; Marroni & Pandolfi, 2007).

2.1 Permo-Triassic metamorphic records

HT-LP metamorphic Permo-Triassic imprints are widely recorded in the Austroalpine and Southalpine continental crust. They are rarely detected in the Penninic crust of Western Alps, and never in the Helvetic domain (Figure 1). These relicts occur in continental crust and mantle rocks and show T-climax mineral assemblages developed under amphibolite and granulite facies conditions (Figure 4a and Table 1 of Supporting Information). T_{max}/P ratio is generally high and suggests thermal conditions characteristic of Barrovian and Abukuma metamorphic field gradients (Figure 4a). Most of the pressure (P) and temperature (T) data lie between the fully relaxed (England & Thompson, 1984) and the near-spreading ridge geotherms (Cloos, 1993), suggesting the occurrence of an extra heat supply with respect to the normal heat generated by radioactive decay after crustal thickening consequent to continental collision (Figure 4a). T_{max}/depth ratios vary from 25 to 50°C/km and, in particular, the maximum ratios rapidly increase from 300 to 270 Ma and gradually decrease up to 220 Ma (Figure 4b). This distribution has been interpreted as the ending of the Permian extensional regime at ca. 260-240 Ma, followed by sag-stage subsidence during slow lithospheric cooling from the Early Triassic (Picazo et al., 2016; Schuster & Stüwe, 2008). No relation occurs between T_{max} ages, metamorphic field gradients (Barrovian and Abukuma) and their present-day distribution through the Alps (Figures 5, 6a).

2.2 Permo-Triassic continental gabbros

Permo-Triassic continental gabbros are located in the Austroalpine and Southalpine domains of the whole Alpine realm (Figure 2) and are associated with subcontinental peridotites emplaced at different structural levels (Figure 4c and Table 2 of Supporting Information) (Bonin et al., 1993; McCarthy & Muntener, 2015; Rottura et al., 1998; Spalla et al., 2014; Spiess, Cesare, Mazzoli, Sassi, & Sassi, 2010; Staehle et al., 2001). Although the gabbros are generally considered to be generated from variably contaminated mantle sources in an extensional tectonic regime under a high thermal state, associated with lithospheric thinning and rifting (Spalla et al., 2014, and refs therein), from a geochemical point of view, most of the gabbros have a tholeitic signature (Spalla et al., 2014, and refs therein). The peridotites contain clino-pyroxene and spinel with Cr content between 20 and 40% (McCarthy & Muntener, 2015; Muntener, Manatschal, Desmurs, & Pettke, 2010; Nicot, 1977). Such a high Cr content of spinel suggests that Permo-Triassic gabbros result from >10% near-fractional melting of peridotites (Hellebrand, Snow, Dick, & Hofmann, 2001; McCarthy & Muntener, 2015). Experimental results on melt compositions and mantle melting percentage at different PT conditions, allow to estimate a maximum pressure of partial melting during Permo-Triassic at 1.5 GPa (Jaques & Green, 1980; Winter, 2003). Continental gabbros show a broad range of radiometric ages, from 300 to 220 Ma, and no relation between ages and the present-day geographic location occurs (Figure 6b).

2.3 Sedimentary basins and volcanics

Three cycles of sedimentary successions and volcanics emplacement have been described from the lower Permian to Jurassic (see extended review in Marotta et al., 2009; Spalla et al., 2014). The first volcano-sedimentary cycle (lower Permian) is characterized by a widespread volcanic activity in the whole Southalpine domain and part of the Helvetic and Penninic domains (Bussy, Sartori, & Thélin, 1996; Cannic, Lapierre, Monié, Briqueu, & Basile, 2001; Maino, Dallagiovanna, Gaggero, Seno, & Tiepolo, 2012), associated with continental clastic deposits (from conglomerates to siltites, Bargossi, Rottura, Vernia, Visonà, & Tranne, 1998; Bussien, Bussy, Masson, Magna, & Rodionov, 2008; Cadel, Cosi, Pennacchioni, & Spalla, 1996; Cassinis & Perotti, 1994, 2007; Dallagiovanna, Gaggero, Maino, Seno, & Tiepolo, 2009; Gretter, Ronchi, Langone, & Perotti, 2013; Maino, Dallagiovanna, Gaggero, Seno, & Tiepolo, 2012; Quick et al., 2009; Visonà, Fioretti, Poli, Zanferrari, & Fanning, 2007). Oldest volcanic products are 291 Ma-old andesites in the northern Dolomites (Visonà et al., 2007), 285-282 Ma-old volcanics in the Southalpine basins of the Central Alps (Zanoni & Spalla, 2018), and 291-285 Ma-old relict lamprophyre in the Antigorio nappe rocks of the Penninic domain of the western Alps (Bussien et al., 2008). The Athesian Platform (Adige/Etsch valley and Dolomites region) is the largest calc-alkaline volcanic and subvolcanic complex of the Southern Alps dated at 280-277 Ma (Schaltegger & Brack, 2007). Locally, two volcanic events are distinguished within the lower Permian volcano-clastic cycle in the Central Alps (Cassinis & Perotti, 1994, 2007; Gretter et al., 2013). The Permian sedimentation is found south and southeast of the Argentera massif in the Helvetic domain (Faure-Muret, 1955). Magmatism and clastic sedimentation in the intracontinental basins have supposed to be originated during large-scale strike-slip transtensional tectonics associated with crustal thinning, upwelling and partial melting of mantle, and advection of melts and heat into the crust (Schaltegger & Brack, 2007) during the transition from the lower Permian Pangea-B to the Late Permian Pangea-A (Muttoni et al., 2003; Muttoni, Erba, Kent, & Bachtadse, 2005). Dextral strike-slip tectonics related to the subduction of Paleotethys ridge has been proposed by (Gretter et al., 2013) to explain the developed of continental basins and intense magmatism during the lower Permian. The origin of the Permian sedimentary troughs in the Southalpine domain may be interpreted as the result of the initial stages of the Tethyan rifting (Siletto, Spalla, Tunesi, Lardeaux, & Colombo, 1993; Winterer & Bosellini, 1981; Zanoni & Spalla, 2018).

A second cycle of volcanics emplacement and shallow-water to marine deposits occurred from the Anisian to Norian in the Southalpine domain (Bernoulli, Bertotti, & Froitzheim, 1990; Bertotti, Picotti, Bernoulli, & Castellarin, 1993; Doglioni, 1987; Gillcrist, Coward, & Mugnier, 1987; Lemoine & Trümpy, 1987; Venturini, 1983). The easternmost sector of the Southalpine domain displays the most continuous tectono-sedimentary record, from the Carboniferous to Triassic. Three changes in the sedimentary sequence are observed and they are interpreted as derived from alternating transpressional and transtensional regime and fault-controlled ground-level fluctuations (Venturini, 1991). Triassic basaltic shoshonites documented in the Dolomites were interpreted as derived from a mantle contaminated by a previous subduction (Sloman, 1989) or transpressional to compressive tectonics (Castellarin, Lucchini, Rossi, Selli, & Simboli, 1988; Doglioni, 1984). However, the generalized subsidence, the lateral variations in thickness of sedimentary successions, and the deepening upward of the facies support the occurrence of extensional tectonics in the Southalpine domain during the Triassic (Carminati et al., 2010). Furthermore, syn-sedimentary normal faults of Triassic age can be detected in the Dolomites (e.g., Doglioni & Carminati, 2008). In the Helvetic domain of the Western Alps, east-dipping Triassic listric faults are responsible for the deposition of syn-rift sediments with interbedded basalts in half-graben structures (Gillcrist et al., 1987; Lemoine & Trümpy, 1987).

The third cycle of sedimentation started from early Jurassic (ca. 185 Ma, Berra, Galli, Reghellin, Torricelli, & Fantoni, 2009), and is associated with the major rifting stage that evolved in the opening of the Alpine Tethys Ocean (Berra et al., 2009).

2.4 Jurassic ophiolites

In the Alps, the transition from rifting to oceanic spreading is marked by the deposition of post-rift sediments (172-165 Ma, Baumgartner et al., 1995; Bill, O'Dogherty, Guex, Baumgartner, & Masson, 2001; Handy et al., 2010; Stampfli et al., 1998) and by the exhumation and serpentinization of subcontinental and ocean-continent transition zone mantle (Figure 3; e.g., Desmurs, Manatschal, & Bernoulli, 2001; Manatschal, 2004; Manatschal & Müntener, 2009; Picazo et al., 2016; Rampone et al., 2014; Tribuzio, Garzetti, Corfu, Tiepolo, & Renna, 2016). The radiometric ages of the oceanic gabbros and peridotites (Figure 6a and Table 3 of Supporting Information) cluster around approximately 160 Ma (Li, Faure, Lin, & Manatschal, 2013; Mevel, Caby, & Kienast, 1978; Riccardo Tribuzio et al., 2016), with older values of 166-183 Ma from the Apennines, Corsica and Erro-Tobbio ophiolitic units (Li, Faure, Rossi, Lin, & Lahondère, 2015; Rampone et al., 2014; R. Tribuzio, 2004). Oldest ages of 198±22 (Sm-Nd on gabbro) have been obtained by Costa & Caby (2001) in ophiolites from the Western Alps (Chenaillet) and interpreted by the authors as the signature of lithospheric extension announcing the oceanic spreading. However, Li et al. (2013) presented new age for the Chenaillet at ca. 165 Ma.

3 NUMERICAL MODELING

We here review the results obtained from two numerical models that simulate the evolution of the Pangea lithosphere from late-collisional evolution of the Variscan chain (Marotta et al., 2009) to the Jurassic opening of the Alpine Tethys (Marotta et al., 2018). The first model (Permo-Triassic extension - MOD1, Marotta et al., 2009) accounts for the evolution of a thermally and mechanically perturbed lithosphere after 70 Myr the end of the Variscan collision (ca. 360 Ma, Franke, 2000; Lardeaux et al., 2014; Matte, 2001; von Raumer et al., 2013), i.e. from 290 to 220 Ma (Marotta et al., 2009). The second model (Jurassic rifting and oceanization - MOD2, Marotta et al., 2018) accounts for the rifting of a mechanically unperturbed continental lithosphere until the crustal break-up and the formation of the oceanic crust (Marotta et al., 2018). The two models have independent initial conditions, and the initial lithospheric structure of MOD2 is not affected by previous events. Therefore, it predicts the evolution of the rifting only considering the thermal perturbation of the lithosphere, and not the presence of mechanical heterogeneities inherited by MOD1. We compare model predictions with geological data from Permo-Triassic metamorphic and intrusive rocks from the Alps and Jurassic ophiolites from the Alps and the Northern Apennines.

3.1 Model setup

The numerical models were performed by using SubMar code (Marotta, Spelta, & Rizzetto, 2006) and successive versions (Marotta et al., 2018; Regorda, Roda, Marotta, & Spalla, 2017; M. Roda et al., 2012). The dynamics of the crust-mantle system were investigated by numerical integration of the three fundamental equations of conservation of mass, momentum and energy, which include the Extended Boussinesq approximation (e.g., Christensen & Yuen, 1985) for incompressible fluids. The numerical code uses the penalty function formulation to integrate the equation for the conservation of momentum and the streamline upwind Petrov-Galerkin method (used to integrate the equation for the conservation of energy). The marker in-cell technique was used to compositionally differentiate crust and mantle rocks. A viscous-plastic behavior was assumed for all materials (Marotta et al., 2006). The material parameters are listed in Table 1. In both models, boundary conditions are defined in terms of velocity and temperature. A temperature of 300 K (ca. 27°C) is fixed at the top of the crust and 1600 K (ca. 1330°C) is fixed at the base of the model (Figure 7). Zero flux is assumed through the lateral sides of the model. Velocity boundary conditions and initial thermal structures vary in the two models and are presented in the following sections.

3.2 Permo-Triassic extension - MOD1

MOD1 lasts 70 Myr, from 290 to 220 Ma. The initial configuration accounts for the temperatures and material distribution obtained after 2500 km of oceanic subduction from 425 to 362.5 Ma (e.g., Tait, Bachtadse, Franke, & Soffel, 1997; von Raumer, Stampfli, & Bussy, 2003), followed by continental collision and a post-collisional gravitational evolution that lasts 72.5 Ma (Marotta et al., 2009). Four different boundary conditions are tested for this model to quantify the influence of the extension rate on the thermo-mechanical setting. An extension rate of 0 cm/yr is used to simulate a late-orogenic gravitational collapse without any far-field forcing (mode 1 collapse, Rey, Vanderhaeghe, & Teyssier, 2001). In the other cases, extension rates of 0.5, 1 and 2 cm/yr, respectively, are applied at the right boundary (mode 2 collapse, Rey et al., 2001) through the crustal thickness of the upper plate (from 0 to 30 km depth). Here, the largest amount of subducted crustal material occurs and therefore it represents the favored location for the occurrence of the Permo-Triassic extension and metamorphism (Marotta et al., 2009) and zero normal stress is assumed from 30 to 80 km depth (Figure 7a,b).

We compare the thermal state predicted by the four simulations with the thermal state suggested by Permo-Triassic PT estimates documented in the Alps. In particular, we plot T_{max}/depth estimates inferred from metamorphic rocks of the Alpine continental crust against the geotherms predicted from the simulations for 70 Myr of evolution (Figure 8). For each output time, we extract the geotherms along the vertical section characterized by highest thermal gradient. For the simulation with an extension rate of 0 cm/yr, the fitting between predictions and geological data is obtained for few T_{max} only (Figure 8a). The fitting for simulations with forced extension increases with the extension rate (Figure 8b,c,e). For an extension rate of 2 cm/yr most of the T_{max}/depth estimates overlap the simulated geotherms (Figure 8d), suggesting a good agreement with the thermal state of Alpine continental lithosphere during the Permo-Triassic. However, some T_{max}/depth estimates remain higher than the simulated geotherms. This simulation shows an increase in the thermal state (warmer geotherms) for 30-35 Myr (i.e., from 290 to 260 Ma) and a subsequent gradual thermal relaxation until 70 Myr (i.e., from 260 to 220 Ma), albeit the forced extension remains constant during the entire simulation.

The most peculiar character of the Permo-Triassic igneous activity is the widespread emplacement of tholeitic and olivine-tholeitic gabbro stocks at different structural levels in the continental crust (Figure 4c), and the occurrence of basaltic products (see Table 4 in Marotta et al., 2009). Therefore, we verify whether the thermal state of the lithospheric mantle predicted by different Ve configurations allows the partial melting of peridotite. When the partial melting occurs, we infer the melting percentage. For each time step, the maximum melt fraction (Mf) of the mantle is calculated on the basis of the parametrized melting model from Katz, Spiegelman, & Langmuir (2003):

$$Mf = \left(\frac{T - T_{solidus}}{T_{liquidus}^{lherz} - T_{solidus}}\right)^{1.5} \rightarrow T > T_{solidus}$$

where T is the temperature of an element belonging to the lithospheric mantle, $T_{liquidus}^{lherz}$ is the temperature of the lherzolite liquidus and $T_{solidus}$ is the temperature of a wet solidus of an enriched peridotite with 0.2% bulk water contents. The latter is compatible with a post-collisional mantle variably contaminated by continental subduction and partially hydrated by Variscan oceanic subduction. Although predictions from the four Ve configurations satisfy the thermal state for mantle partial melting, only the simulation with extension rate of 2 cm/yr produces mantle partial melting >10% (Figure 9). This amount of partial melting is reached after 10 Myr of forced extension and persists until the end of the simulation (70 Myr), reaching a maximum value of 15-17%.

The final thermo-mechanical setting is very different between the four Ve configurations. In the gravitational simulation (Ve=0 cm/yr) both the crustal thickness and the lithospheric thermal state are similar to the initial conditions, while in the forced extension simulations (Ve=0.5, 1 and 2 cm/yr) a strong lithospheric thinning associated with a hot thermal state occurs (Marotta et al., 2009). Localization of maximum shear strain in the gravitational simulation occurs at the crust-mantle interface and mainly under a compressional regime (Figure 10a,c,e). On the contrary, in the forced extension simulations shear strain localization occurs through the entire crust and under an extensional regime (Figure 10b,d,f). The localization of strain occurs cyclically with a periodicity between 10 and 5 Myr (Marotta et al., 2009).

3.3 Jurassic rifting and oceanization - MOD2

MOD2 accounts for the transition from rifting to oceanization and lasts 45 Myr. The model includes the hydration of the uprising mantle peridotite (Table 1) and a constant extension rate fixed to 1.25 cm/yr on both sides of the domain through the crustal thickness, resulting in total extension rate of 2.5 cm/yr, compatible with the magma-poor nature of the rift (Manatschal & Müntener, 2009). Shear-free conditions are prescribed along the top and the bottom boundaries and a sticky air material is included above the crust in order to model vertical movement of the topographic surface. Both crust and lithospheric mantle markers are allowed to exit the model domain since zero normal stress is assumed along vertical boundaries. A weak seed is placed at crust-mantle interface to focus the rifting at the center of the computational domain. Two different thermal settings of the lithosphere represent the initial conditions: a hot and thin lithosphere, characterized by the 1600 K (ca. 1330°C) isotherm located at 80 km depth, and a cold and thick lithosphere, with the 1600 K isotherm located at 220 km depth (Figure 7c). The two configurations result from two different interpretations of the pre-Alpine evolution of the lithosphere. The first one accounts for a thermally perturbed lithosphere consequent to the Permo-Triassic extension (e.g., Marotta & Spalla, 2007; Marotta et al., 2009; Spalla et al., 2014), while the second one is consequent to a Triassic phase of thermal and mechanical requilibration (Picazo et al., 2016; Schuster & Stüwe, 2008).

On the basis of the setup, the model results in a symmetric rifting of the continental lithosphere and shows the exhumation of a serpentinized lithospheric mantle (ocean-continent transition zone - OCTZ) for both simulations (Figure 11). However, the onset of the lithospheric thinning strongly depends on the initial lithospheric thermal state (see

Figure 3 in Marotta et al., 2018): for a cold and thick (i.e., strong) lithosphere, the thinning is very rapid (4.4 Myr) with respect to a hot and thin (i.e., weak) lithosphere (15.4 Myr). Similarly, the occurrence of the crustal break-up is faster for a cold lithosphere (7.4 Myr) than for a hot lithosphere (approximately 31.4 Myr). For both initial thermal configurations of the lithosphere, the exhumation of the serpentinized mantle starts before the oceanic spreading and mantle partial melting, making the model compatible with a magma-poor rifting, as suggested for the Alpine case (e.g., Manatschal, Lavier, & Chenin, 2015). For the hot configuration the thickness of the continental crust sensibly decreases during the extension from 30 km to approximately 5 km close to the OCTZ. For the cold configuration instead, the crustal thickness decreases from 30 km to approximately 20 km (see Figure 3 in Marotta et al., 2018).

In order to verify whether the thermal state predicted by the two simulations can result in the partial melting of the mantle and the formation of the oceanic lithosphere, we estimate the time and melting percentage of the lithospheric mantle during the rifting. As for MOD1, the melt fraction is still calculated based on the parametrized melting model from (Katz et al., 2003), but taking into account a dry solidus of a depleted peridotite. We assume that mantle partial melting and oceanic lithosphere start simultaneously. Both simulations result in a melting fraction >20%, typical for basaltic melts (Winter, 2003), but at two different time steps. For a hot and thin lithosphere it occurs after 38 Myr, while for a cold and thick lithosphere after 24 Myr (Figure 12). Both simulations match the emplacement PT conditions and paleogeographic setting of oceanic gabbros exposed in the Alps (Table 3 of the Supporting Information), as demonstrated by (Marotta et al., 2018).
In addition, considering that a hyperextended system was assumed to the Alpine Tethys rifting (e.g., Manatschal et al., 2015) and that the emplacement of oceanic gabbros (ca. 160-170 Ma, see review in Marotta et al., 2018, 2009) occurred approximately 35-40 Myr after the first extensional structures related to the rifting event (200 Ma, Mohn, Manatschal, Beltrando, Masini, & Kusznir, 2012), we indicate that a rifting developing on thermally perturbed lithosphere better agrees the natural data.

4 DISCUSSION

The thermal state predicted by a model of forced lithospheric extension (MOD 1) fits well with the thermal state extrapolated from the review of metamorphic and intrusives rocks of Permo-Triassic age (Figure 8). This correspondence enforces the interpretation of a regional extensional tectonics that characterized the lithosphere of Pangea during the Permo-Triassic, causing the asthenospheric upwelling and lithospheric thinning (Diella et al., 1992; Lardeaux & Spalla, 1991; Marotta et al., 2009; Muntener & Hermann, 2001; Schuster & Stüwe, 2008; Spalla et al., 2014; Spalla & Marotta, 2007). In particular, an extension rate of at least 2 cm/yr generates a thermal state in agreement with most T_{max}/depth estimates obtained from Permo-Triassic metamorphic rocks (Figure 8d). Notably, in this simulation (Ve 2 cm/yr) the thermal state (T_{max}/depth ratio) increases within the first 30-35 Myr (from 290 to 260 Ma) and then gradually decreases up to the end of the simulation (70 Myr, 220 Ma). A similar trend is shown by the T_{max}/depth ratio extrapolated from metamorphic rocks. T_{max}/depth ratio shows a rapid increase from 300 to 270-260 Ma and a successive gradual decrease up to 220 Ma (Figure 4b). This distribution was previously interpreted as the result of a Permian extensional regime active until ca. 260-240 Ma, followed by sag-stage subsidence active during slow lithospheric cooling from the Early Triassic (Picazo et al., 2016; Schuster & Stüwe, 2008). In this review we demonstrate that the variation in the thermal state of the lithosphere from 290 to 220 Ma can be explained even by a model of continuous extension from the Permian to Triassic. In this model, the long-lasting extension does not result in the continental break-up but rather in a uniform thinning of the lithosphere.

Within a continuous extensional regime, cyclic variation in the localization of shear strain may occur through the entire crust with a periodicity of about 10 Myr (Marotta et al., 2009). This periodicity can be interpreted as a local variation in the tectonic regime that affects the crust or can be related to the free-slip condition imposed for the top boundary of the domain that precludes vertical movement of the crust.

In the whole Southalpine domain widespread volcanic activity characterized the Permian time. In the Dolomites and Carnia, Early to Middle Triassic sediments host dykes and pillow basaltic lavas. The sedimentary sequences record periodic continental-marine transition during the lower Permian and at the Permo-Triassic boundary in the. Dextral strike-slip faulting with an extensional component is compatible with Permian tectonic history, although minor sinistral effects are recorded in the Dolomites. In any cases, there is general consensus in connecting the Permian calc-alkaline magmatism with the lithospheric thinning and strike-slip tectonics (Bergomi, Dal Piaz, Malusà, Monopoli, & Tunesi, 2017; Dallagiovanna et al., 2009; Schaltegger & Brack, 2007).

Extension starts prevailing on strike-slip displacement since the Triassic. The Triassic volcanics products in the Dolomites have a mainly calc-alkaline affinity and have been interpreted as deriving from the melting of a mantle contaminated by a previous subduction (Sloman, 1989) or as the result of crustal contamination of mafic melts. Alternatively, the calc-alkaline volcanics are interpreted as produced in a back-arc region during the final stages of the Paleotethys subduction (Muttoni et al., 2015). However, the lack of Triassic high-pressure rocks in the Alpine region does not support the presence of an oceanic subduction.

Numerical modeling indicates that these cyclic periods of active extension and tectonic stasis leading the formation of basins in the upper crust and volcanics emplacement at the surface, can be explained by the cyclic variation in the localization of shear strain during a continuous extension. The localization of the shear strain in discrete shear zones could accommodate the subsidence of upper crust basins and allow the ascent of magma (and related volcanics products) from deep-seated mafic intrusions and their consequent contamination with crustal material.

In the Alpine region, the Permo-Triassic period is also characterized by a widespread igneous activity with intrusion of large gabbro bodies through the continental crust. Radiometric ages show a broad range of intrusion time, from ca. 300 to ca. 220 Ma, and no relation between emplacement age and present-day geographic location can be inferred (Figure 6b). Generally, basic intrusions have a tholeitic and olivine-tholeitic geochemical signature (Spalla et al., 2014) and derives from 10-20% partial melting of peridotites (Hellebrand et al., 2001; McCarthy & Muntener, 2015) occurred at depth <50km (Jaques & Green, 1980; Winter, 2003). This means that the lithosphere must have been hot enough to produce tholeitic gabbros during the entire Permian and Triassic period. A simulation with continuous extension of 2 cm/yr satisfies this condition, resulting in a potential mantle melting >10% for almost 60 Myr, from 280 to 220 Ma (Figure 9).

The model of rifting (MOD2) of a thermally perturbed lithosphere (i.e., hot, thin and weak, Marotta et al., 2018) results in a hyperextended system with the first emplacement of oceanic gabbros after 35 Myr from the start of the extension (Figure 11). This scenario fits with the hyperextended nature of the Alpine Tethys rifting (Manatschal et al., 2015) as well as the time span existing between the first extensional structures related to the rifting (ca.

200 Ma, Mohn et al., 2012) and the emplacement of oceanic gabbros (ca. 170-160 Ma, Marotta et al., 2018, 2009). Therefore, a thermally perturbed lithosphere can better represent the lithosphere of Pangea at ca. 200 Ma. In addition, the good fitting existing between geological data and model predictions of post-collisional extension and the ages of HT-LP metamorphic rocks and continental gabbros emplacement, clearly indicate the persistence of a high thermal state of the lithosphere from the Permian until 230-220 Ma (Figures 4, 5, 6). The duration of igneous activity in the Ivrea-Verbano Zone further supports this interpretation (Klötzli et al., 2014; Langone et al., 2017; Peressini, Quick, Sinigoi, Hofmann, & Fanning, 2007; Schaltegger et al., 2015; Zanetti et al., 2016). Furthermore, a time span of 20-30 Myr (from 230 to 200 Ma) is a too short period to complete the thermo-mechanical requilibration of the lithosphere. In contrast with the rifting model (MOD2), the post-collisional model (MOD1) does not result in the continental break-up and this is mainly due to the heterogeneity that characterize the lithosphere of the MOD1 which would represent the heritage of the Variscan subduction and collision. This thermo-mechanical setting results in a slower lithosphere thinning. Furthermore, lack of a weak seed in the model setup leads a rather uniform extension of the lithosphere. The ophiolites of the Alps and Apennines have an age younger than 175 Ma (Fig. 6a), that is in agreement with the emplacement time of the oceanic gabbros in the model with a thermally perturbed lithosphere (>40 Myr from the start of the extension, i.e. <180 Ma).

The Permo-Triassic HT-LP metamorphic rocks and the gabbro bodies are concentrated in the Austroalpine and Southalpine domains and lack in the Helvetic domain (Figures 1, 2), supporting the interpretation of an asymmetric rifting (e.g., Lardeaux & Spalla, 1991; Marotta et al., 2009). On the contrary, in the presented review, the model (MOD2) simulates the extension of a homogeneous lithosphere resulting in a symmetric rifting. However, a rifting developed on heterogeneous lithosphere and upper mantle characterized by structures inherited from previous tectonics events (i.e., Variscan subduction and collision), can be strongly asymmetric (e.g., Manatschal et al., 2015; Marotta et al., 2009; Petersen & Schiffer, 2016; Spalla et al., 2014) even if the far field extension is symmetrically applied on both margins.

We propose that after the Variscan orogeny, a long-lasting extensional tectonics, starting in the Permian (ca. 290-300 Ma), resulted in the Mesozoic rifting and breaking of Pangea supercontinent (Figure 13). This tectonic context can explain the Permo-Triassic high thermal regime and the opening of the Alpine Tethys as a hyperextended magma-poor margin. This process can be characterized by alternated periods of active extension and tectonic stasis in the upper crust until the formation of the ocean, as proposed for the Northern Atlantic rifting (Doré & Stewart, 2002) or as envisaged for the Ivrea-Verbano Zone (as documented by three metamorphic ages, Permian, Triassic and Jurassic; Langone & Tiepolo, 2015). The strong structural asymmetry resulting from the thermal and mechanical perturbation induced by the convergence-related processes related to the Variscan orogeny in the whole upper mantle, can lead the occurrence of an asymmetric rifting of Pangea in the Alpine region.

5 CONCLUSIONS

The review of Permo-Triassic to Jurassic geological data from the Alps and the Northern Apennines and the predictions of two existing numerical models that simulate the evolution of the lithosphere from the late collisional events of the Variscan orogeny to the Jurassic opening of the Alpine Tethys supports the interpretation of an Alpine Tethys rifting and oceanization developed on a lithosphere characterized by a thermo-mechanical configuration consequent to a post-Variscan extension, which affected Pangea during the Permian and Triassic. Therefore, a long-lasting period of continuous active extension (2 cm/yr) can be envisaged for the breaking of Pangea, starting from the unrooting of the Variscan belts (ca. 300 Ma), followed by the Permo-Triassic thermal peak (as suggested by HT-LP metamorphism and emplacement of gabbros), and ending with the crustal break-up and the formation of the Alpine Tethys Ocean (ca. 170-160 Ma). This continuous process of lithospheric extension leaded to thinning and break-up of Pangea through the occurrence of cyclic periods of active extension and tectonic stasis in the upper continental crust, until the formation of the oceanic crust. On the other hand, PT estimates from the rocks exhumed from the pre-Alpine lower crust indicate the persistence of a high T/P ratio at deep structural level from the Permian to Jurassic.

The occurrence of a heterogeneous lithosphere and a strongly thermally and mechanically perturbed upper mantle inherited from Variscan convergence promoted the development of an asymmetric rifting, as suggested by the concentration of Permo-Triassic HT metamorphic rocks and gabbro bodies in the southern margin of the Alpine Tethys.

Acknowledgments

We gratefully acknowledge the Editor Chiara Frassi and two anonymous reviewers for their highly constructive suggestions that greatly improved the early version of the text. This work was supported by Linea 2, Azione A - fondi giovani ricercatori "Geodinamica delle zone attive della litosfera" (PSR2017-DZANONI).

References

Arcay, D., Tric, E., & Doin, M.-P. (2005). Numerical simulations of subduction zones. *Physics of the Earth and Planetary Interiors*, *149*(1–2), 133–153. https://doi.org/10.1016/j.pepi.2004.08.020

Arthaud, F., & Matte, P. (1977). Late Paleozoic strike-slip faulting in southern Europe and northern Africa: Result of a right-lateral shear zone between the Appalachians and the Urals. *Geological Society of America Bulletin*, *88*(9), 1305. https://doi.org/10.1130/0016-7606(1977)88<1305:LPSFIS>2.0.CO;2

Bargossi, G. M., Rottura, A., Vernia, L., Visonà, D., & Tranne, C. A. (1998). Guida all'escursione sul distretto vulcanico atesino e sulle plutoniti di Bressanone- Chiusa e Cima d'Asta. *Memorie Della Società Geologica Italiana*, *53*, 23–41.

Baumgartner, P. O., Bartolini, A., Carter, E. S., Conti, M., Cortese, G., Danelian, T., … Yao, A. (1995). Middle Jurassic to Early Cretaceous radiolarian biochronology of Tethys based on Unitary Associations. In: "Middle Jurassic to Lower Cretaceous Radiolaria of Tethys: Occurrences, Systematics, Biochronology." *Memoires de Geologie (Lausanne, Switzerland) Edited by: InterRad Jurassic-Cretaceous Working Group,23*, 1013–1048.

Beardsmore, G. R., & Cull, J. P. (2001). *Crustal Heat Flow: aguide to measurement and modelling*. Cambridge University Press.

Bergomi, M. A., Dal Piaz, G. V., Malusà, M. G., Monopoli, B., & Tunesi, A. (2017). The Grand St Bernard-Briançonnais Nappe System and the Paleozoic Inheritance of the Western Alps Unraveled by Zircon U-Pb Dating. *Tectonics*, *36*(12), 2950–2972. https://doi.org/10.1002/2017TC004621

Bernoulli, D., Bertotti, G., & Froitzheim, N. (1990). Mesozoic faults and associated sediments in the Austroalpine-south alpine passive continental margin. *Memorie Della Società Geologica Italiana*, *45*, 25–38.

Berra, F., Galli, M. T., Reghellin, F., Torricelli, S., & Fantoni, R. (2009). Stratigraphic evolution of the Triassic-Jurassic succession in the Western Southern Alps (Italy): the record of the two-stage rifting on the distal passive margin of Adria. *Basin Research*, *21*(3), 335–353. https://doi.org/10.1111/j.1365-2117.2008.00384.x

Bertotti, G., Picotti, V., Bernoulli, D., & Castellarin, A. (1993). From rifting to drifting: tectonic evolution of the South-Alpine upper crust from the Triassic to the Early Cretaceous. *Sedimentary Geology*, *86*(1–2), 53–76. https://doi.org/10.1016/0037-0738(93)90133-P

Bertotti, G., Siletto, G. B., & Spalla, M. I. (1993). Deformation and metamorphism associated with crustal rifting: The Permian to Liassic evolution of the Lake Lugano-Lake Como area (Southern Alps). *Tectonophysics*, *226*(1–4), 271–284. https://doi.org/10.1016/0040-1951(93)90122-Z

Best, M. G., & Christiansen, E. H. (2001). *Igneous Petrology*. Blackwell Sci., London.

Bill, M., O'Dogherty, L., Guex, J., Baumgartner, P. O., & Masson, H. (2001). Radiolarite ages in Alpine-Mediterranean ophiolites: Constraints on the oceanic spreading and the Tethys-Atlantic connection. *Geological Society of America Bulletin*, *113*(1), 129–143. https://doi.org/10.1130/0016-7606(2001)113

Bonin, B., Brändlein, P., Bussy, F., Desmons, J., Eggenberger, U., Finger, F., … Vivier, G. (1993). Late Variscan Magmatic Evolution of the Alpine Basement. In *Pre-Mesozoic Geology in the Alps* (pp. 171–201). Berlin, Heidelberg: Springer Berlin Heidelberg. https://doi.org/10.1007/978-3-642-84640-3_11

Bousquet, R., Engi, M., Gosso, G., Oberhänsli, R., Berger, A., Spalla, M. I., … Goffè, B. (2004). Explanatory notes to the map: metamorphic structure of the Alps transition from the Western to the Central Alps. *Mitteilungen Der Gesellschaft Der Geologie-*

Und Bergbaustudenten in Österreich, *149*, 145–156.

Brack, P. (1981). Structures in the southwestern border of the Adamello intrusion (Alpi Bresciane, Italy). *Schweizerische Mineralogische Und Petrographische Mitteilungen*, *61*, 37–50. https://doi.org/10.5169/seals-47129

Bussien, D., Bussy, F., Masson, H., Magna, T., & Rodionov, N. (2008). Variscan lamprophyres in the Lower Penninic domain (Central Alps): age and tectonic significance. *Bulletin de La Société Géologique de France*, *179*(4). https://doi.org/10.2113/gssgfbull.179.4.369

Bussy, F., Sartori, M., & Thélin, P. (1996). U-Pb zircon dating in the middle Penninic basement of the Western Alps (Valais, Switzerland). *Schweizerische Mineralogische Und Petrographische Mitteilungen*, *76*, 81–84. https://doi.org/10.5169/seals-57689

Cadel, G., Cosi, M., Pennacchioni, G., & Spalla, M. I. (1996). A new map of the Permo-Carboniferous cover and Variscan metamorphic basement in the Central Orobic Alps, Southern Alps - Italy. *Memorie Di Scienze Geologiche, Padova*, *48*, 1–53.

Cannic, S., Lapierre, H., Monié, P., Briqueu, L., & Basile, C. (2001). Late orogenic evolution of the Variscan lithosphere: Nd isotopic constraints from the Western Alps. *Schweizerische Mineralogische Und Petrographische Mitteilungen*, *82*, 77–99.

Carminati, E., Cavazza, D., Scrocca, D., Fantoni, R., Scotti, P., & Doglioni, C. (2010). Thermal and tectonic evolution of the southern Alps (northern Italy) rifting: Coupled organic matter maturity analysis and thermokinematic modeling. *AAPG Bulletin*, *94*(3), 369–397. https://doi.org/10.1306/08240909069

Carminati, E., & Doglioni, C. (2012). Alps vs. Apennines: The paradigm of a tectonically asymmetric Earth. *Earth-Science Reviews*, *112*(1–2), 67–96. https://doi.org/10.1016/j.earscirev.2012.02.004

Cassinis, G., & Perotti, C. R. (1994). Interazione strutturale permiana tra la linea delle Giudicarie ed i bacini di Collio, Tione e Tregiovo (Sudalpino centrale, N Italia). *Bollettino Della Societa Geologica Italiana*, *112*, 1021–1036.

Cassinis, G., & Perotti, C. R. (2007). A stratigraphic and tectonic review of the Italian Southern Alpine Permian. *Palaeoworld*, *16*(1), 140–172. https://doi.org/10.1016/j.palwor.2007.05.004

Castellarin, A., Lucchini, F., Rossi, P. L., Selli, L., & Simboli, G. (1988). The Middle Triassic magmatic-tectonic arc development in the Southern Alps. *Tectonophysics*, *146*, 79–89.

Chopra, P. N., & Paterson, M. S. (1981). The experimental deformation of dunite. *Tectonophysics*, *78*(1–4), 453–473. https://doi.org/10.1016/0040-1951(81)90024-X

Christensen, U. R., & Yuen, D. A. (1985). Layered convection induced by phase transitions. *Journal of Geophysical Research*, *90*(B12), 10291–10300. https://doi.org/10.1029/JB090iB12p10291

Cloos, M. (1993). Lithospheric buoyancy and collisional orogenesis: Subduction of oceanic plateaus, continental margins, island arcs, spreading ridges, and seamounts. *Geological Society of America Bulletin*, *105*(6), 715. https://doi.org/10.1130/0016-7606(1993)105<0715:LBACOS>2.3.CO;2

Costa, S., & Caby, R. (2001). Evolution of the Ligurian Tethys in the Western Alps: Sm/Nd and U/Pb geochronology and rare-earth element geochemistry of the Montgenèvre ophiolite (France). *Chemical Geology*, *175*(3–4), 449–466. https://doi.org/10.1016/S0009-2541(00)00334-X

Dal Piaz, G. V. (2010). The Italian Alps: a journey across two centuries of Alpine geology. *Journal of the Virtual Explorer*, *36*(8). https://doi.org/10.3809/jvirtex.2010.00234

Dallagiovanna, G., Gaggero, L., Maino, M., Seno, S., & Tiepolo, M. (2009). U-Pb zircon ages for post-Variscan volcanism in the Ligurian Alps (Northern Italy). *Journal of the Geological Society*, *166*(1), 101–114. https://doi.org/10.1144/0016-76492008-027

Delleani, F., Rebay, G., Zucali, M., Tiepolo, M., Spalla, M. I., (2018). Insights on Variscan geodynamics from the structural and geochemical characterization of a Devonian-Carboniferous gabbro from the Austroalpine Domain (Western Alps). *Ofioliti* 43, 23–29. https://doi.org/10.4454/ofioliti.v43i1.454.

Desmons, J., Compagnoni, R., Cortesogno, L., Frey, M., & Gaggero, L. (1999). Pre-Alpine metamorphism of the Internal zones of the Western Alps. *Schweizerische Mineralogische Und Petrographische Mitteilungen*, *79*, 23–39. https://doi.org/10.5169/seals-60196

Desmurs, L., Manatschal, G., & Bernoulli, D. (2001). The Steinmann Trinity revisited: mantle exhumation and magmatism along an ocean-continent transition: the Platta nappe, eastern Switzerland. *Geological Society, London, Special Publications*, *187*(1), 235–266. https://doi.org/10.1144/GSL.SP.2001.187.01.12

Diella, V., Spalla, M. I., & Tunesi, A. (1992). Contrasting thermomechanical evolutions in the Southalpine metamorphic basement of the Orobic Alps (Central Alps, Italy). *Journal of Metamorphic Geology*, *10*(2), 203–219. https://doi.org/10.1111/j.1525-1314.1992.tb00079.x

Doglioni, C. (1984). Tettonica triassica transpressiva nelle Dolomiti. *Giornale Di Geologia*, *46/2*, 47–60.

Doglioni, C. (1987). Tectonics of the Dolomites (southern alps, northern Italy). *Journal of Structural Geology*, *9*(2), 181–193. https://doi.org/10.1016/0191-8141(87)90024-1

Doglioni, C., & Carminati, E. (2008). Structural styles and Dolomites field trip. In *Memorie descrittive della Carta Geologica d'Italia Volume LXXXII* (p. 301). APAT - Agenzia per la protezione dell'ambiente e per i servizi tecnici d'Italia, Servizio Geologico.

Donatio, D., Marroni, M., & Rocchi, S. (2013). Serpentinization history in mantle section from a fossil slow-spreading ridge sequence/ evidences from Pomaia quarry (Southern Tuscany, Italy). *Ofioliti*, *38*(1), 15–28. https://doi.org/10.4454/ofioliti.v38i1.413

Doré, A. G., & Stewart, I. C. (2002). Similarities and differences in the tectonics of two passive margins : the Northeast Atlantic Margin and the Australian North West Shelf. In M. Keep & S. J. Moss (Eds.), *The Sedimentary Basins of Western Australia 3* (pp. 89–117). Petroleum Exploration Society of Australia (PESA).

Dubois, J., & Diament, M. (1997). *Géophysique*. Masson, Paris.

England, P. C., & Thompson, A. B. (1984). Pressure--Temperature--Time Paths of Regional Metamorphism I. Heat Transfer during the Evolution of Regions of Thickened Continental Crust. *Journal of Petrology*, *25*(4), 894–928. https://doi.org/10.1093/petrology/25.4.894

Faure-Muret, A. (1955). Etudes géologiques sur le massif de l'Argentera-Mercantur. In *Mémoires du Service de la Carte Géologique de la France* (p. 336). Imprimerie Nationale.

Franke, W. (2000). The mid-European segment of the Variscides: tectonostratigraphic units, terrane boundaries and plate tectonic evolution. *Geological Society, London, Special Publications*, *179*(1), 35–61. https://doi.org/10.1144/GSL.SP.2000.179.01.05

Gardien, V., Reusser, E., & Marquer, D. (1994). Pre-Alpine metamorphic evolution of the gneisses from the Valpelline series (Western Alps, Italy). *Schweizerische Mineralogische Und Petrographische Mitteilungen*, *74*, 489–502. https://doi.org/10.5169/seals-56364

Gillcrist, R., Coward, M., & Mugnier, J.-L. (1987). Structural inversion and its controls : examples from the Alpine foreland and the French Alps. *Geodinamica Acta*, *1*(1), 5–34. https://doi.org/10.1080/09853111.1987.11105122

Gretter, N., Ronchi, A., Langone, A., & Perotti, C. R. (2013). The transition between the two major Permian tectono-stratigraphic cycles in the central Southern Alps: results from facies analysis and U/Pb geochronology. *International Journal of Earth Sciences*, *102*(5), 1181–1202. https://doi.org/10.1007/s00531-013-0886-4

Handy, M. R., Schmid, S. M., Bousquet, R., Kissling, E., & Bernoulli, D. (2010). Reconciling plate-tectonic reconstructions of Alpine Tethys with the geological--geophysical record of spreading and subduction in the Alps. *Earth-Science Reviews*, *102*, 121–158. https://doi.org/10.1016/j.earscirev.2010.06.002

Hellebrand, E., Snow, J. E., Dick, H. J. B., & Hofmann, A. W. (2001). Coupled major and trace elements as indicators of the extent of melting in mid-ocean-ridge peridotites. *Nature*, *410*(6829), 677–681. https://doi.org/10.1038/35070546

Honda, S., & Saito, M. (2003). Small-scale convection under the back-arc occurring in the low viscosity wedge. *Earth and Planetary Science Letters*, *216*(4), 703–715. https://doi.org/10.1016/S0012-821X(03)00537-5

Jaques, A. L., & Green, D. H. (1980). Anhydrous melting of peridotite at 0-15 Kb pressure and the genesis of tholeiitic basalts. *Contributions to Mineralogy and Petrology*, *73*(3), 287–310. https://doi.org/10.1007/BF00381447

Katz, R. F., Spiegelman, M., & Langmuir, C. H. (2003). A new parameterization of hydrous mantle melting. *Geochemistry, Geophysics, Geosystems*, *4*(9), 1–19. https://doi.org/10.1029/2002GC000433

Klötzli, U. S., Sinigoi, S., Quick, J. E., Demarchi, G., Tassinari, C. C. G., Sato, K., & Günes, Z. (2014). Duration of igneous activity in the Sesia Magmatic System and implications for high-temperature metamorphism in the Ivrea–Verbano deep crust. *Lithos*, *206–207*(0), 19–33. https://doi.org/10.1016/j.lithos.2014.07.020

Langone, A., Padrón-Navarta José, A., Ji, W.-Q., Zanetti, A., Mazzucchelli, M., Tiepolo, M., … Bonazzi, M. (2017). Ductile-brittle deformation effects on crystal-chemistry and U-Pb ages of magmatic and metasomatic zircons from a dyke of the Finero Mafic Complex (Ivrea-Verbano Zone, Italian Alps). *Lithos*, *284–285*, 493–511. https://doi.org/10.1016/j.lithos.2017.04.020

Langone, A., & Tiepolo, M. (2015). U-Th-Pb “multi-phase” approach to the study of crystalline basement: application to the northernmost sector of the Ivrea-Verbano Zone (Alps). *Periodico Di Mineralogia*, *84*(3B), 633–655. https://doi.org/10.2451/2015PM0435

Lardeaux, J.-M. (2014). Deciphering orogeny: a metamorphic perspective. Examples from European Alpine and Variscan belts: Part I: Alpine metamorphism in the western Alps. A review. *Bulletin de La Societe Geologique de France*, *185*(2), 93–114. https://doi.org/10.2113/gssgfbull.185.2.93

Lardeaux, J. M., Schulmann, K., Faure, M., Janoušek, V., Lexa, O., Skrzypek, E., … Štípská, P. (2014). The Moldanubian Zone in the French Massif Central, Vosges/Schwarzwald and Bohemian Massif revisited: differences and similarities. *Geological Society, London, Special Publications*, *405*(1), 7–44. https://doi.org/10.1144/SP405.14

Lardeaux, J. M., & Spalla, M. I. (1991). From granulites to eclogites in the Sesia zone (Italian Western Alps): a record of the opening and closure of the Piedmont ocean. *Journal of Metamorphic Geology*, *9*(1), 35–59. https://doi.org/10.1111/j.1525-1314.1991.tb00503.x

Lemoine, M., & Trümpy, R. (1987). Pre-oceanic rifting in the alps. *Tectonophysics*, *133*(3–4), 305–320. https://doi.org/10.1016/0040-1951(87)90272-1

Li, X.-H., Faure, M., Lin, W., & Manatschal, G. (2013). New isotopic constraints on age and magma genesis of an embryonic oceanic crust: The Chenaillet Ophiolite in the Western Alps. *Lithos*, *160–161*, 283–291. https://doi.org/10.1016/j.lithos.2012.12.016

Li, X.-H., Faure, M., Rossi, P., Lin, W., & Lahondère, D. (2015). Age of Alpine Corsica ophiolites revisited: Insights from in situ zircon U–Pb age and O–Hf isotopes. *Lithos*, *220–223*(0), 179–190. https://doi.org/10.1016/j.lithos.2015.02.006

Maino, M., Dallagiovanna, G., Gaggero, L., Seno, S., & Tiepolo, M. (2012). U-Pb zircon geochronological and petrographic constraints on late to post-collisional Variscan magmatism and metamorphism in the Ligurian Alps, Italy. *Geological Journal*, *47*(6), 632–652. https://doi.org/10.1002/gj.2421

Malatesta, C., Crispini, L., Federico, L., Capponi, G., & Scambelluri, M. (2012). The exhumation of high pressure ophiolites (Voltri Massif, Western Alps): Insights from structural and petrologic data on metagabbro bodies. *Tectonophysics*, *568*, 102–123. https://doi.org/10.1016/j.tecto.2011.08.024

Malatesta, C., Gerya, T., Crispini, L., Federico, L., & Capponi, G. (2013). Oblique subduction modelling indicates along-trench tectonic transport of sediments. *Nature Communications*, *4*, 1–6. https://doi.org/10.1038/ncomms3456

Manatschal, G. (2004). New models for evolution of magma-poor rifted margins based on a review of data and concepts from West Iberia and the Alps. *International Journal of Earth Sciences*, *93*(3), 432–466. https://doi.org/10.1007/s00531-004-0394-7

Manatschal, G., Lavier, L., & Chenin, P. (2015). The role of inheritance in structuring hyperextended rift systems: Some considerations based on observations and numerical modeling. *Gondwana Research*, *27*(1), 140–164. https://doi.org/10.1016/j.gr.2014.08.006

Manatschal, G., & Müntener, O. (2009). A type sequence across an ancient magma-poor ocean–continent transition: the example of the western Alpine Tethys ophiolites. *Tectonophysics*, *473*(1–2), 4–19. https://doi.org/10.1016/j.tecto.2008.07.021

Marotta, A. M., Roda, M., Conte, K., & Spalla, M. I. (2018). Thermo-mechanical numerical model of the transition from continental rifting to oceanic spreading: the case study of the Alpine Tethys. *Geological Magazine*, *155*(02), 250–279. https://doi.org/10.1017/S0016756816000856

Marotta, A. M., & Spalla, M. I. (2007). Permian-Triassic high thermal regime in the Alps: Result of late Variscan collapse or continental rifting? Validation by numerical modeling. *Tectonics*, *26*(4), 1–30. https://doi.org/10.1029/2006TC002047

Marotta, A. M., Spalla, M. I., & Gosso, G. (2009). Upper and lower crustal evolution during lithospheric extension: numerical modelling and natural footprints from the European Alps. In U. Ring & B. Wernicke (Eds.), *Extending a Continent: Architecture, Rheology and Heat Budget.* (Vol. 321, pp. 33–72). The Geological Society, London, Special Publications. https://doi.org/10.1144/SP321.3

Marotta, A. M., Spelta, E., & Rizzetto, C. (2006). Gravity signature of crustal subduction inferred from numerical modelling. *Geophys. J. Int.*, *166*, 923–938. https://doi.org/10.1111/j.1365-246X.2006.03058.x

Marroni, M., Molli, G., Ottri, G., & Pandolfi, L. (2001). Tectono-sedimentary evolution of the External Liguride units (Northern Apennines, Italy): insights in the pre-collisional history of a fossil ocean-continent transition zone. *Geodinamica Acta*, *14*(5), 307–320. https://doi.org/10.1016/S0985-3111(00)01050-0

Marroni, M., & Pandolfi, L. (2007). The architecture of an incipient oceanic basin: a tentative reconstruction of the Jurassic Liguria-Piemonte basin along the Northern Apennines--Alpine Corsica transect. *International Journal of Earth Sciences*, *96*(6), 1059–1078. https://doi.org/10.1007/s00531-006-0163-x

Matte, P. (2001). The Variscan collage and orogeny (480-290 Ma) and the tectonic definition of the Armorica microplate: a review. *Terra Nova*, *13*(2), 122–128. https://doi.org/10.1046/j.1365-3121.2001.00327.x

McCarthy, A., & Muntener, O. (2015). Ancient depletion and mantle heterogeneity: Revisiting the Permian-Jurassic paradox of Alpine peridotites. *Geology*, *43*(3), 255–258. https://doi.org/10.1130/G36340.1

Mevel, C., Caby, R., & Kienast, J.-R. (1978). Amphibolite facies conditions in the oceanic crust: example of amphibolitized flaser-gabbro and amphibolites from the Chenaillet ophiolite massif (Hautes Alpes, France). *Earth and Planetary Science Letters*, *39*(1), 98–108. https://doi.org/10.1016/0012-821X(78)90146-2

Mohn, G., Manatschal, G., Beltrando, M., Masini, E., & Kusznir, N. (2012). Necking of continental crust in magma-poor rifted margins: Evidence from the fossil Alpine Tethys margins. *Tectonics*, *31*(1), 1–28. https://doi.org/10.1029/2011TC002961

Muntener, O., & Hermann, J. (2001). The role of lower crust and continental upper mantle during formation of non-volcanic passive margins: evidence from the Alps. *Geological Society, London, Special Publications*, *187*(1), 267–288. https://doi.org/10.1144/GSL.SP.2001.187.01.13

Muntener, O., Manatschal, G., Desmurs, L., & Pettke, T. (2010). Plagioclase Peridotites in Ocean-Continent Transitions: Refertilized Mantle Domains Generated by Melt Stagnation in the Shallow Mantle Lithosphere. *Journal of Petrology*, *51*(1–2), 255–294. https://doi.org/10.1093/petrology/egp087

Muttoni, G., Erba, E., Kent, D. V., & Bachtadse, V. (2005). Mesozoic Alpine facies deposition as a result of past latitudinal plate motion. *Nature*, *434*(7029), 59–63. https://doi.org/10.1038/nature03378

Muttoni, G., Kent, D. V, Garzanti, E., Brack, P., Abrahamsen, N., & Gaetani, M. (2003). Early Permian Pangea 'B' to Late Permian Pangea 'A'☆. *Earth and Planetary Science Letters*, *215*(3–4), 379–394. https://doi.org/10.1016/S0012-821X(03)00452-7

Muttoni, G., Tartarotti, P., Chiari, M., Marieni, C., Rodelli, D., Dallanave, E., & Kirscher, U. (2015). Paleolatitudes of Late Triassic radiolarian cherts from Argolis, Greece: Insights on the paleogeography of the western Tethys. *Palaeogeography, Palaeoclimatology, Palaeoecology*, *417*, 476–490. https://doi.org/10.1016/j.palaeo.2014.10.010

Neubauer, F., Frisch, W., Schmerold, R., & Schlöser, H. (1989). Metamorphosed and dismembered ophiolite suites in the basement units of the Eastern Alps. *Tectonophysics*, *164*(1), 49–62. https://doi.org/10.1016/0040-1951(89)90233-3

Nicot, E. (1977). *Les roches meso and catazonales de la Valpelline (nappe de la Dent Blanche; Alpes Italiennes)*. Universite´ Pierre et Marie Curie, Paris VI.

Peressini, G., Quick, J. E., Sinigoi, S., Hofmann, A. W., & Fanning, M. (2007). Duration of a Large Mafic Intrusion and Heat Transfer in the Lower Crust: a SHRIMP U-Pb Zircon Study in the Ivrea-Verbano Zone (Western Alps, Italy). *Journal of Petrology*, *48*(6), 1185–1218. https://doi.org/10.1093/petrology/egm014

Petersen, K. D., & Schiffer, C. (2016). Wilson cycle passive margins: Control of orogenic inheritance on continental breakup. *Gondwana Research*, *39*, 131–144. https://doi.org/10.1016/j.gr.2016.06.012

Picazo, S., Müntener, O., Manatschal, G., Bauville, A., Karner, G., & Johnson, C. (2016). Mapping the nature of mantle domains in Western and Central Europe based on clinopyroxene and spinel chemistry: Evidence for mantle modification during an extensional cycle. *Lithos*, *266*, 233–263. https://doi.org/10.1016/j.lithos.2016.08.029

Piqué, A., & Laville, E. (1996). The central Atlantic rifting: Reactivation of Palaeozoic structures? *Journal of Geodynamics*, *21*(3), 235–255. https://doi.org/10.1016/0264-3707(95)00022-4

Platt, J. P. (1986). Dynamics of orogenic wedges and the uplift of high-pressure metamorphic rocks. *Geological Society of America Bulletin*, *97*(9), 1037. https://doi.org/10.1130/0016-7606(1986)97<1037:DOOWAT>2.0.CO;2

Polino, R., Dal Piaz, G. V, & Gosso, G. (1990). Tectonic erosion at the Adria margin and accretionary processes for the Cretaceous orogeny of the Alps. *Mémoires de La Societé Géologique de France*, *156*, 345–367.

Quick, J. E., Sinigoi, S., Peressini, G., Demarchi, G., Wooden, J. L., & Sbisà, A. (2009). Magmatic plumbing of a large Permian caldera exposed to a depth of 25 km. *Geology*, *37*, 603–606. https://doi.org/10.1130/G30003A.1

Rampone, E., Borghini, G., Romairone, A., Abouchami, W., Class, C., & Goldstein, S. L. (2014). Sm-Nd geochronology of the Erro-Tobbio gabbros (Ligurian Alps, Italy): Insights into the evolution of the Alpine Tethys. *Lithos*, *205*, 236–246. https://doi.org/10.1016/j.lithos.2014.07.012

Ranalli, G., & Murphy, D. C. (1987). Rheological stratification of the lithosphere. *Tectonophysics*, *132*(4), 281–295. https://doi.org/10.1016/0040-1951(87)90348-9

Regorda, A., Roda, M., Marotta, A. M., & Spalla, M. I. (2017). 2-D numerical study of hydrated wedge dynamics from subduction to post-collisional phases. *Geophysical Journal International*, *211*(2), 952–978. https://doi.org/10.1093/gji/ggx336

Rey, P., Vanderhaeghe, O., & Teyssier, C. (2001). Gravitational collapse of the continental crust: definition, regimes and modes. *Tectonophysics*, *342*(3–4), 435–449. https://doi.org/10.1016/S0040-1951(01)00174-3

Roda, M., Marotta, A. M., & Spalla, M. I. (2010). Numerical simulations of an ocean-continent convergent system: Influence of subduction geometry and mantle wedge hydration on crustal recycling. *Geochemistry, Geophysics, Geosystems*, *11*(5). https://doi.org/10.1029/2009GC003015

Roda, M., Marotta, A. M., & Spalla, M. I. (2010). Numerical simulations of an ocean-continent convergent system: Influence of subduction geometry and mantle wedge hydration on crustal recycling. *Geochemistry, Geophysics, Geosystems*, *11*(5), 1–21. https://doi.org/10.1029/2009GC003015

Roda, M., Spalla, M. I., & Marotta, A. M. (2012). Integration of natural data within a numerical model of ablative subduction: a possible interpretation for the Alpine dynamics of the Austroalpine crust. *Journal of Metamorphic Geology*, *30*(9), 973–996. https://doi.org/10.1111/jmg.12000

Rottura, A., Bargossi, G. M., Caggianelli, A., Del Moro, A., Visonà, D., & Tranne, C. A. (1998). Origin and significance of the Permian high-K calc-alkaline magmatism in the central-eastern Southern Alps, Italy. *Lithos*, *45*(1–4), 329–348. https://doi.org/10.1016/S0024-4937(98)00038-3

Rybach, L. (1988). Determination of heat production rate. In *Handbook of terrestrial heat-flow density determination* (pp. 125–142). Solid Earth Sciences Library, Kluwer Academic Publishers.

Sandiford, M., & Powell, R. (1986). Deep crustal metamorphism during continental extension: modern and ancient examples. *Earth and Planetary Science Letters*, *79*(1–2), 151–158. https://doi.org/10.1016/0012-821X(86)90048-8

Schaltegger, U., & Brack, P. (2007). Crustal-scale magmatic systems during intracontinental strike-slip tectonics: U, Pb and Hf isotopic constraints from Permian magmatic rocks of the Southern Alps. *International Journal of Earth Sciences*, *96*(6), 1131–1151. https://doi.org/10.1007/s00531-006-0165-8

Schaltegger, U., Ulianov, A., Müntener, O., Ovtcharova, M., Peytcheva, I., Vonlanthen, P., … Girlanda, F. (2015). Megacrystic zircon with planar fractures in miaskite-type nepheline pegmatites formed at high pressures in the lower crust (Ivrea Zone, southern Alps, Switzerland). *American Mineralogist*, *100*(1), 83–94.

Schuster, R., & Stüwe, K. (2008). Permian metamorphic event in the Alps. *Geology*, *36*, 603–606. https://doi.org/10.1130/G24703A.1

Siletto, G. B., Spalla, M. I., Tunesi, A., Lardeaux, J. M., & Colombo, A. (1993). Pre-Alpine Structural and Metamorphic Histories in the Orobic Southern Alps, Italy. In *Pre-Mesozoic Geology in the Alps* (pp. 585–598). Berlin, Heidelberg: Springer Berlin Heidelberg. https://doi.org/10.1007/978-3-642-84640-3-34

Sloman, L. E. (1989). Triassic shoshonites from the Dolo- mites, Northern Italy: alkaline arc rocks in a strike- slip setting. *Journal of Geophysical Research*, *94*, 4655–4666.

Spalla, M. I., Gosso, G., Marotta, A. M., Zucali, M., & Salvi, F. (2010). Analysis of natural tectonic systems coupled with numerical modelling of the polycyclic continental lithosphere of the Alps. *International Geology Review*, *52*(10–12), 1268–1302. https://doi.org/10.1080/00206814.2010.482737

Spalla, M. I., Lardeaux, J. M., Piaz, G. vittorio D., Gosso, G., & Messiga, B. (1996). Tectonic significance of Alpine eclogites. *Journal of Geodynamics*, *21*(3), 257–285. https://doi.org/10.1016/0264-3707(95)00033-X

Spalla, M. I., & Marotta, A. M. (2007). P-T evolutions vs. numerical modelling: a key to unravel the Paleozoic to early-Mesozoic tectonic evolution of the Alpine area. *Periodico Di Mineralogia*, *76*(2–3), 267–308. https://doi.org/10.2451/2007PM0029

Spalla, M. I., Zanoni, D., Marotta, A. M., Rebay, G., Roda, M., Zucali, M., & Gosso, G. (2014). The transition from Variscan collision to continental break-up in the Alps: insights from the comparison between natural data and numerical model predictions. *Geological Society, London, Special Publications*, *405*(1), 363–400. https://doi.org/10.1144/SP405.11

Spiess, R., Cesare, B., Mazzoli, C., Sassi, R., & Sassi, F. P. (2010). The crystalline basement of the Adria microplate in the eastern Alps: a review of the palaeostructural evolution from the Neoproterozoic to the Cenozoic. *Rendiconti Lincei*, *21*(S1), 31–50. https://doi.org/10.1007/s12210-010-0100-6

Staehle, V., Frenzel, G., Hess, J. C., Saupe, F., Schmidt, S. T., & Schneider, W. (2001). Permian metabasalt and Triassic alkaline dykes in the northern Ivrea zone: clues to the post-Variscan geodynamic evolution of the Southern Alps. *Schweizerische Mineralogische Und Petrographische Mitteilungen*, *81*, 1–21. https://doi.org/10.5169/seals-61677

Stampfli, G. ., Mosar, J., Marquer, D., Marchant, R., Baudin, T., & Borel, G. (1998). Subduction and obduction processes in the Swiss Alps. *Tectonophysics*, *296*(1–2), 159–204. https://doi.org/10.1016/S0040-1951(98)00142-5

Stöckhert, B., & Gerya, T. V. (2005). Pre-collisional high pressure metamorphism and nappe tectonics at active continental margins: a numerical simulation. *Terra Nova*, *17*, 102–110. https://doi.org/10.1111/j.1365-3121.2004.00589.x

Tait, J. A., Bachtadse, V., Franke, W., & Soffel, H. C. (1997). Geodynamic evolution of the European Variscan fold belt: palaeomagnetic and geological constraints. *Geologische Rundschau*, *86*(3), 585. https://doi.org/10.1007/s005310050165

Thompson, A. B. (1981). The pressure – temperature (P,T) plane viewed by geophysicists and petrologists. *Terra Cognita*, *1*, 11–20.

Tribuzio, R. (2004). Origin of the Gabbro-Peridotite Association from the Northern Apennine Ophiolites (Italy). *Journal of Petrology*, *45*(6), 1109–1124. https://doi.org/10.1093/petrology/egh006

Tribuzio, R., Garzetti, F., Corfu, F., Tiepolo, M., & Renna, M. R. (2016). U–Pb zircon geochronology of the Ligurian ophiolites (Northern Apennine, Italy): Implications for continental breakup to slow seafloor spreading. *Tectonophysics*, *666*, 220–243. https://doi.org/10.1016/j.tecto.2015.10.024

Venturini, C. (1991). Introduction to the geology of the Pramollo Basin (Carnic Alps) and its surroundings. *Giornale Di Geologia*, *53*, 13–47.

Venturini, G. (1983). Il bacino tardo-Ercinico di Pramollo (Alpi Carniche): un’evoluzione regolata dalla tettonica sinsedimentaria. *Memorie Della Società Geologica Italiana*, *24*, 23–42.

Visonà, D., Fioretti, A. M., Poli, M. E., Zanferrari, A., & Fanning, M. (2007). U-Pb SHRIMP zircon dating of andesite from the Dolomite area (NE Italy): geochronological evidence for the early onset of Permian Volcanism in the eastern part of the southern Alps. *Swiss Journal of Geosciences*, *100*(2), 313–324. https://doi.org/10.1007/s00015-007-1219-z

von Raumer, J. F., Bussy, F., Schaltegger, U., Schulz, B., & Stampfli, G. M. (2013). Pre-Mesozoic Alpine basements-Their place in the European Paleozoic framework. *Geological Society of America Bulletin*, *125*(1–2), 89–108. https://doi.org/10.1130/B30654.1

von Raumer, J. F., Stampfli, G. M., & Bussy, F. (2003). Gondwana-derived microcontinents — the constituents of the Variscan and Alpine collisional orogens. *Tectonophysics*, *365*(1–4), 7–22. https://doi.org/10.1016/S0040-1951(03)00015-5

Winter, J. D. (2003). *Principles of Igneous and Metamorphic Petrology*. Pearson Education Limited, Harlow, United Kingdom.

Winterer, E. L., & Bosellini, A. (1981). Subsidence and sedimentation in Jurassic passive continental margin, Southern Alps, Italy. *American Association of Petroleum Geologists Bulletin*, *65*, 394–421.

Zanetti, A., Giovanardi, T., Langone, A., Tiepolo, M., Wu, F.-Y., Dallai, L., & Mazzucchelli, M. (2016). Origin and age of zircon-bearing chromitite layers from the Finero phlogopite peridotite (Ivrea–Verbano Zone, Western Alps) and geodynamic consequences. *Lithos*, *262*, 58–74. https://doi.org/10.1016/j.lithos.2016.06.015

Zanoni, D., & Spalla, M. I. (2018). The Variscan evolution in the basement cobbles of the Permian Ponteranica Formation by microstructural and petrologic analysis. *Italian Journal of Geosciences*, *137*(2), 254–271. https://doi.org/10.3301/IJG.2018.12

Zanoni, D., Spalla, M. I., & Gosso, G. (2010). Structure and PT estimates across late-collisional plutons: constraints on the exhumation of western Alpine continental HP units. *International Geology Review*, *52*(10), 1244–1267. https://doi.org/10.1080/00206814.2010.482357

	Continental crust	Mantle	Serpentiniz. mantle Weak seed	Sticky air
Composition	66% gneiss, 33% granite	100% dunite	100% serpentine	-
Ref. Density [kg/m^3]	2640	3200	3000	1180
Heat product. [10^{-6} W/m^3]	2.5	0.002	0.002	-
Thermal conduct. [W/(mK)]	3.06	4.15	4.15	0.026
Rheology	dry granite	dry dunite	serpentinite	sticky air
Activation energy [kJ/mol]	123	444	-	-
Ref. Viscosity [Pa s]	3.47e^{21}	5.01e^{20}	1e^{19}	1e^{20}
MOD	1-2	1-2	2	2
References	a,b,c	a,b,d	e,b	a,b

Table 1: Material parameters used for the numerical modeling after and Marotta et al. (2018). References: (a) Best & Christiansen (2001); Dubois & Diament (1997); (b) Rybach (1988); (c) Ranalli & Murphy (1987); (d) Chopra & Paterson (1981); (e) Arcay, Tric, & Doin (2005); Honda & Saito (2003); Regorda et al. (2017); Roda, Marotta, & Spalla (2010).

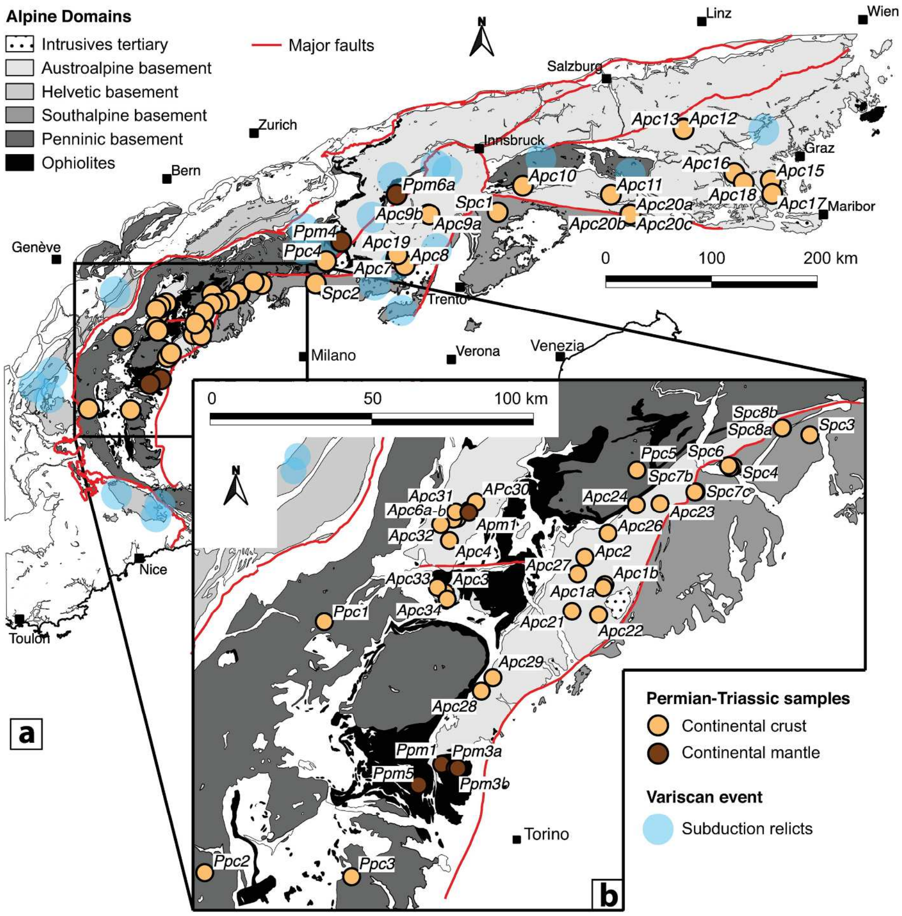

Figure 1 (a) Location of Permo-Triassic metamorphic samples in continental crust and mantle in the Alps. (b) Focus on the Western Alps. Sample codes, geological locations, lithologies, PT estimates, ages (where present) and references are present in Table 1 of Supporting Information.

229x208mm (300 x 300 DPI)

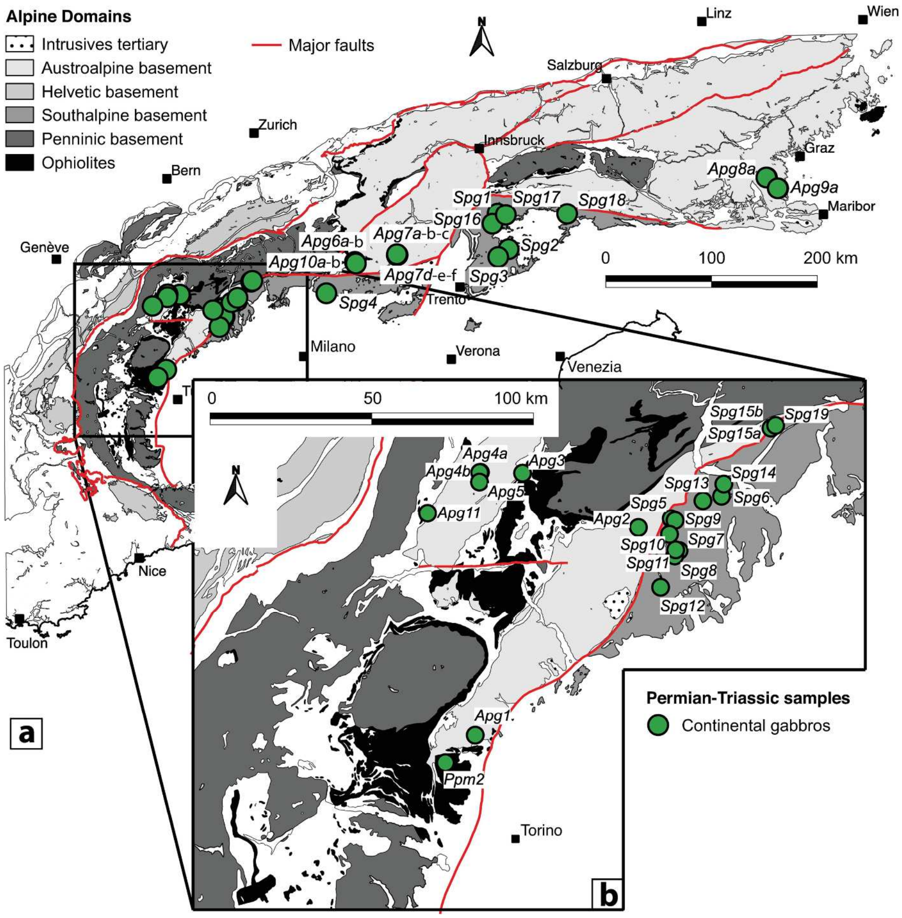

Figure 2 (a) Location of Permo-Triassic continental gabbros in the Alps. (b) Focus on the Western Alps. Sample codes, geological locations, lithologies, PT estimates, ages (where present) and references are present in Table 2 of Supporting Information.

229x208mm (300 x 300 DPI)

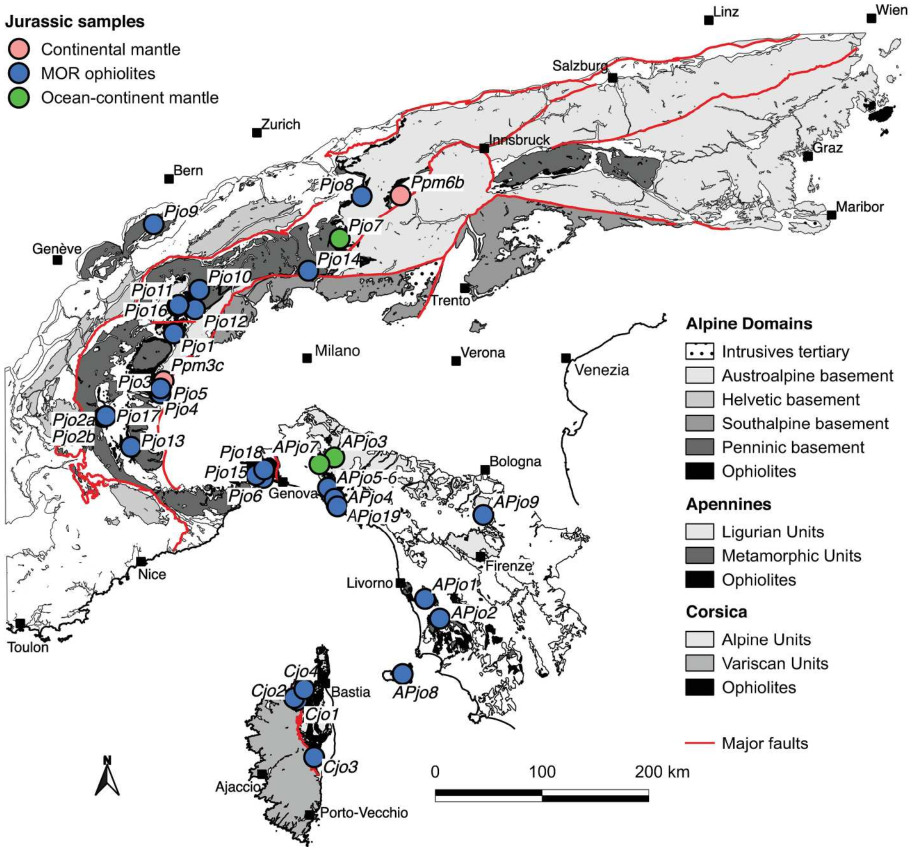

Figure 3 Location and geodynamics setting of Jurassic ophiolites and continental mantle samples in the Alps, Corsica and Northern Apennines. Sample codes, geological locations, lithologies, PT estimates, ages (where present) and references are present in Table 3 of Supporting Information.

210x177mm (300 x 300 DPI)

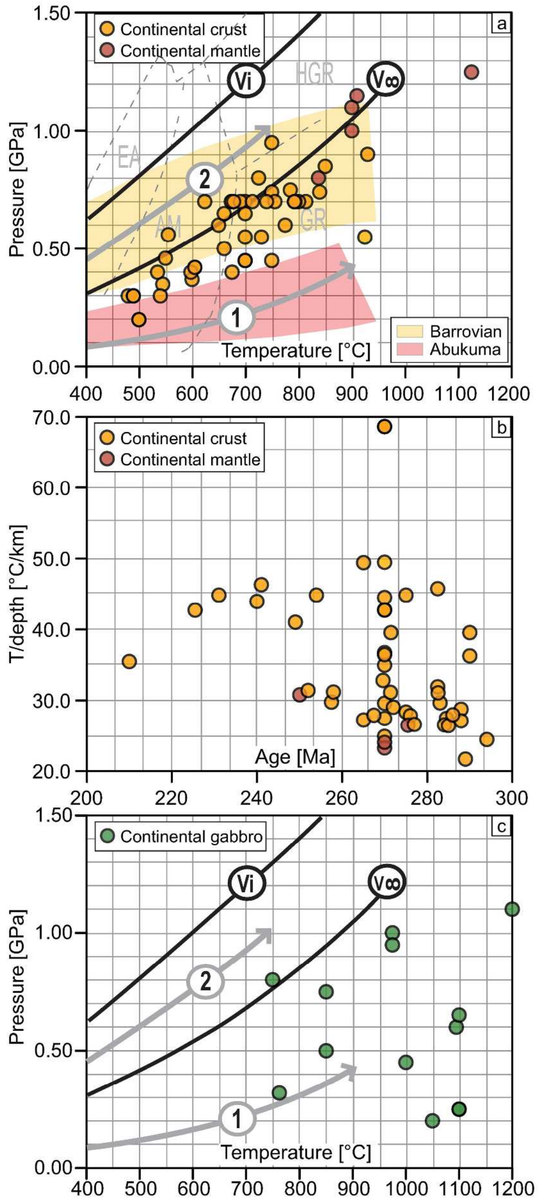

Code	Temp (°C)	Pres (GPa)	Age (Ma)
Continental crust samples			
Ppc2	500.0	0.20	270.0
Ppc1	500.0	0.20	270.0
Ppc3	700.0	0.55	270.0
Apc33	713.0	0.70	286.0
Apc32	740.0	0.70	272.0
Apc3	600.0	0.37	270.0
Apc34	792.5	0.70	282.6
Apc4	545.0	0.35	270.0
Apc6b	750.0	0.45	282.5
Apc31	678.0	0.70	277.0
Apc6a	814.0	0.70	282.5
Apc5	775.0	0.60	210.0
APc30	690.5	0.70	288.0
Apc28	794.0	0.70	271.4
Apc29	673.5	0.70	285.0
Apc21	750.0	0.95	289.0
Apc27	676.0	0.70	284.0
Apc2	700.0	0.65	270.0
Apc1b	700.0	0.70	270.0
Apc1a	725.0	0.80	270.0
Apc26	623.5	0.70	294.0
Ppc5	540.0	0.30	265.0
Apc24	800.0	0.70	252.0
Apc23	756.0	0.70	283.0
Spc7c	840.0	0.74	258.0
Spc7b	750.0	0.74	276.0
Spc6	785.0	0.75	288.0
Spc5	850.0	0.85	284.5
Spc4	730.0	0.55	270.0
Spc2	700.0	0.45	225.5
Ppc4	930.0	0.90	275.0
Apc7	660.0	0.50	290.0
Apc19	925.0	0.55	270.0
Apc8	700.0	0.45	270.0
Apc9a	605.0	0.42	290.0
Apc9b	605.0	0.42	271.5
Spc1	565.0	0.18	272.5
Apc10	650.0	0.60	257.5
Apc11	675.0	0.40	241.0
Apc20b	490.0	0.30	254.0
Apc20a	490.0	0.30	275.0
Apc20c	490.0	0.30	231.0
Apc12	480.0	0.30	240.0
Apc13	535.0	0.40	270.0
Apc16	597.5	0.40	249.0
Apc18	550.0	0.46	269.6
Apc15	555.0	0.56	265.0
Apc17	660.0	0.65	267.5
Continental mantle samples			
Ppm1	1125.0	1.25	275.5
Ppm3a	1000.0	2.05	275.5
Ppm3b	837.5	0.80	250.0
Apm1	900.0	1.00	
Ppm4	910.0	1.15	270.0
Ppm6a	900.0	1.10	270.0
Continental gabbro samples			
Ppm2	1000.0	0.45	275.5
Apg4a	1095.0	0.60	284.0
Apg1	850.0	0.75	272.5
Spg10	1100.0	0.65	248.0
Spg11	750.0	0.80	274.0
Spg15a	975.0	0.95	231.0
Spg4	762.5	0.32	279.0
Apg6a	1200.0	1.10	271.0
Apg7a	850.0	0.50	267.0
Spg1	1050.0	0.20	276.0
Spg2	975.0	1.00	229.5
Apg9b	1100.0	0.25	255.0
Apg9a	1100.0	0.25	247.0

Figure 4 (a) PT conditions of Permo-Triassic metamorphic rocks from the Alps compared to Barrovian and Abukuma metamorphic field gradients and facies (after Ernst and Liou, 2008). Most of the PT data lie between the fully relaxed (2) and the near-spreading ridge (1) geotherms. EA = epidote amphibolite; AM = amphibolite; HGR = high pressure granulite; GR = granulite. Gray lines refer to: (1) near spreading ridge or volcanic arc and (2) normal gradient of old plate interior (Cloos, 1993); Black lines refer to Vi = stable and V∞ = relaxed geotherms for the continental crust (England & Thompson, 1984). (b) T/depth ratio vs age of Permo-Triassic metamorphic crust and mantle samples. The ratios vary from 25 to 50◦C/km and rapidly increase from 300 to 270 Ma and gradually decrease up to 220 Ma. Depths are obtained using a constant density of 2800 kg/m3 for the crust and 3000 kg/m^3 for the mantle, which represent the average values on the basis of the simulated lithostratigraphy. (c) PT conditions of Permo-Triassic gabbros from the Alps. EA = epidote amphibolite; AM = amphibolite; HGR = high pressure granulite; GR = granulite. Gray lines refer to: (1) near spreading ridge or volcanic arc and (2) normal gradient of old plate interior (Cloos, 1993); Black lines refer to Vi = stable and V∞ = relaxed geotherms for the continental crust (England & Thompson, 1984).

235x319mm (300 x 300 DPI)

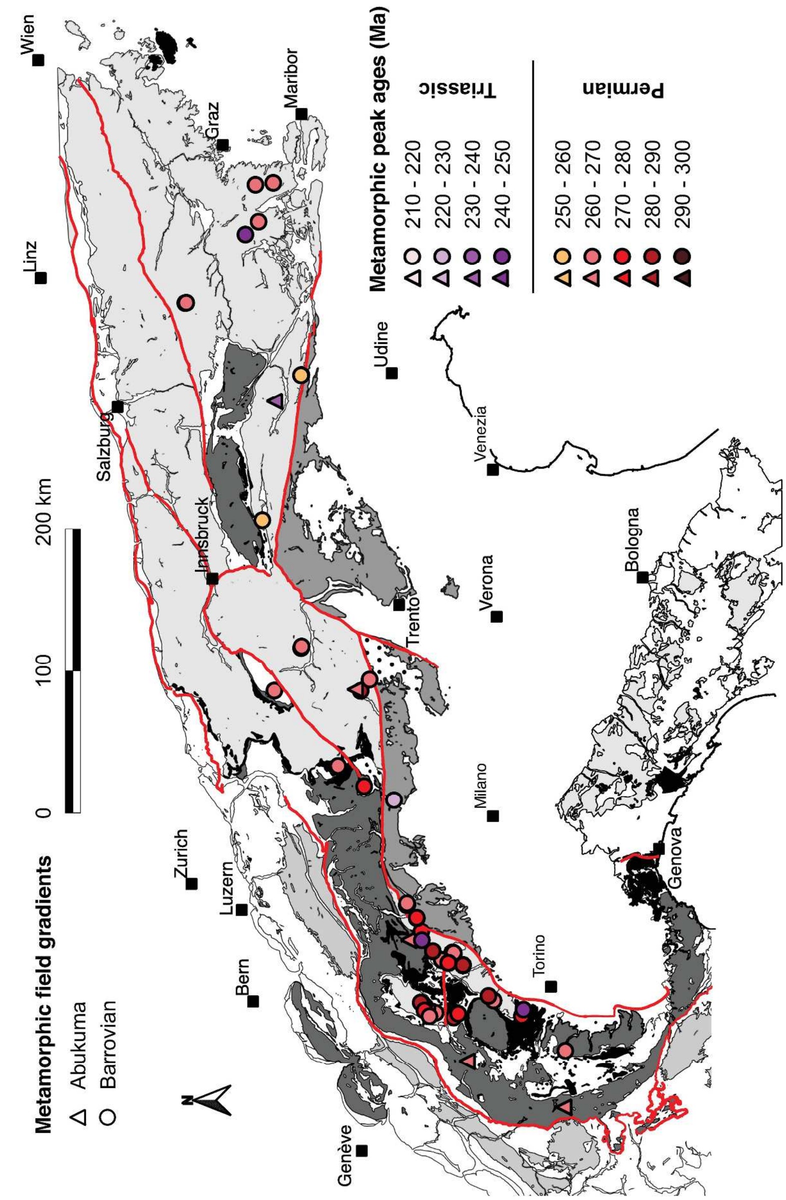

Figure 5 Geographic distribution of metamorphic field gradients (Barrovian and Abukuma) and their Permo-Triassic peak ages in the Alps. No relation occurs between metamorphic field gradients, ages, and their present-day distribution through the Alps.

240x370mm (300 x 300 DPI)

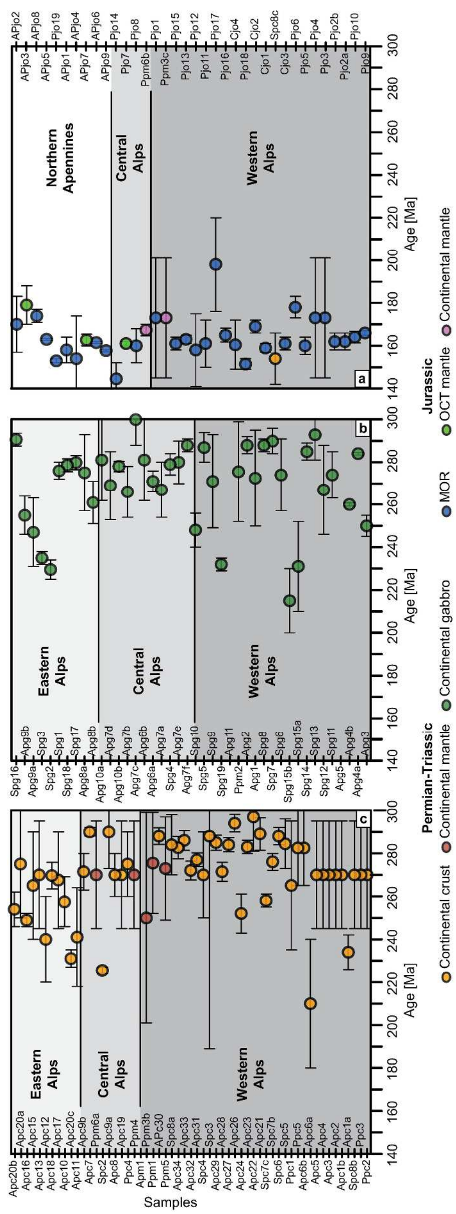

Figure 6 Ages of metamorphic and igneous events recorded in Permo-Triassic metamorphic rocks (a), continental gabbros (b) and ophiolites (c) from the Alps and Northern Apennines. Sample codes, geological locations, lithologies, PT estimates, ages (where present) and references are present in the tables of Supporting Information.

235x630mm (300 x 300 DPI)

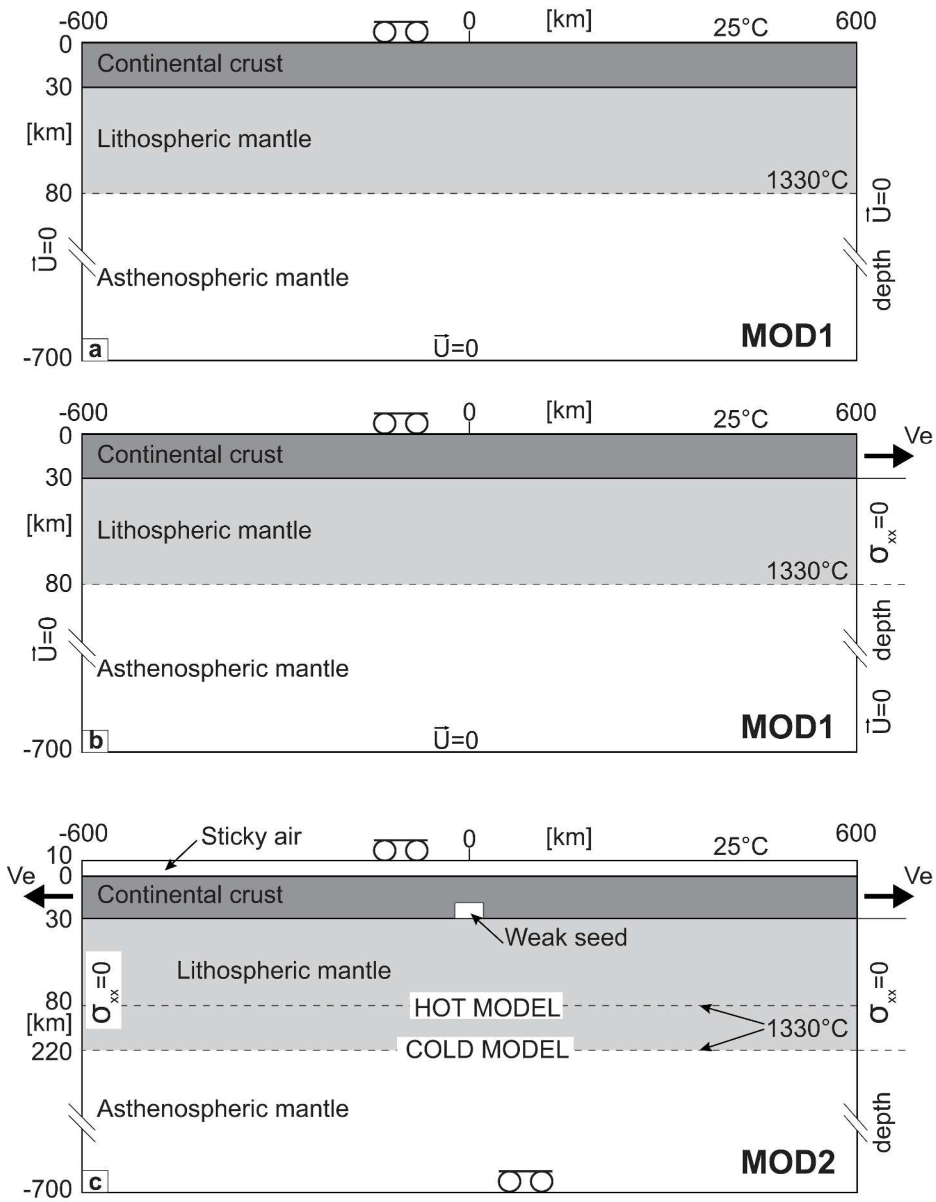

Figure 7 Model setups. (a,b) MOD1 lasts 70 Myr, from 290 to 220 Ma. Different extension rates (Ve) of 0 (a - gravitational collapse), 0.5, 1 and 2 cm/yr (b - forced extension) are applied through the crustal thickness of the upper plate at the right boundary. Zero normal stress (σ_{xx}) is assumed from 30 to 80 km depth along the right boundary while zero velocity ($\vec{U}$) is assumed along the left and bottom boundary. A shear-free condition is applied at the top boundary. Initial thermo-mechanical conditions are obtained after 70 Myr of gravitational re-equilibration at the end of the Variscan subduction and collision. (c) MOD2 lasts 45 Myr. The extension rate (Ve) is constant and fixed to 1.25 cm/yr on both sides of the domain (total extension rate of 2.5 cm/yr) and shear-free conditions are prescribed at the top and the bottom boundaries. Two different initial thermal settings of the lithosphere are considered: a hot and thin lithosphere characterized by 1600 K (ca. 1330◦C) isotherm located at 80 km depth, and a cold and thick lithosphere with 1600 K isotherm located at 220 km depth.

474x614mm (600 x 600 DPI)

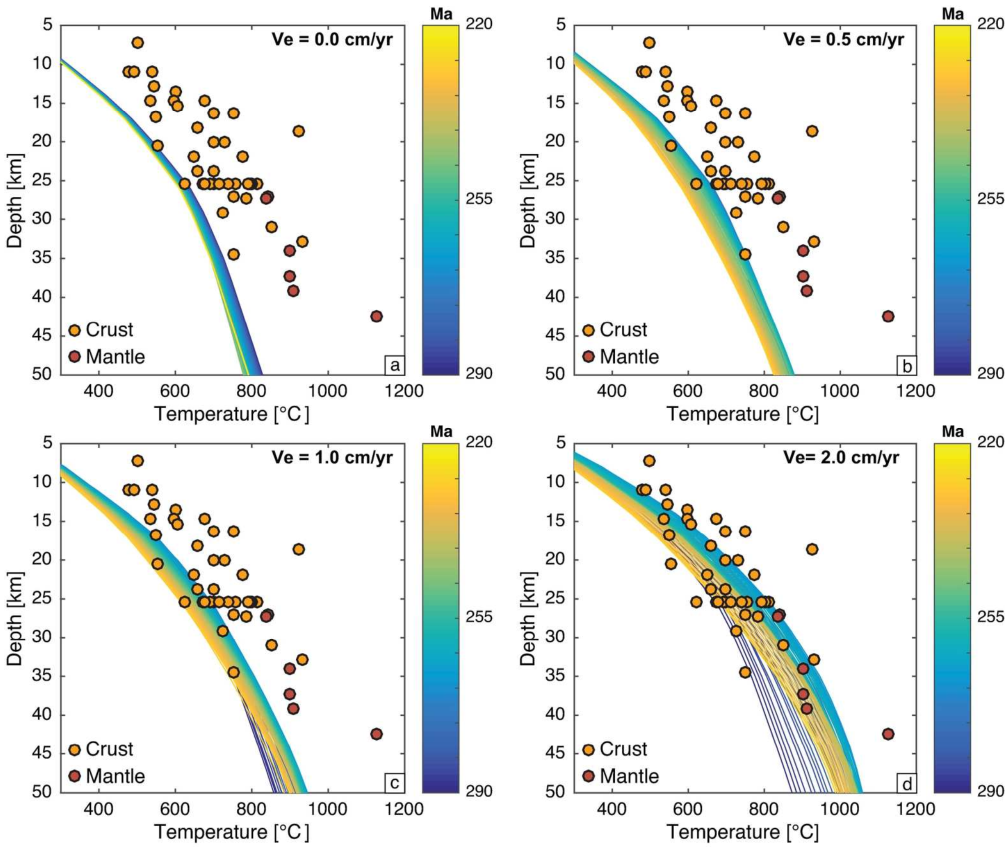

Figure 8 Geotherm curves predicted by MOD1 for 0, 0.5, 1.0 and 2.0 cm/yr extension rates during 290-220 Ma interval, compared to T-depth estimates from Permo-Triassic metamorphic rocks (same samples of Figure 4a,b). We extracted the geotherms along the vertical section characterized by the highest thermal gradient. Depths are obtained using a constant density of 2800 kg/m^3 for the crust and 3000 kg/m^3 for the mantle (i.e. average values on the basis of the simulated lithostratigraphy). For an extension rate of 0 cm/yr, the fitting between predictions and geological data is poor. The best fit occurs for an extension rate of 2 cm/yr.

164x138mm (300 x 300 DPI)

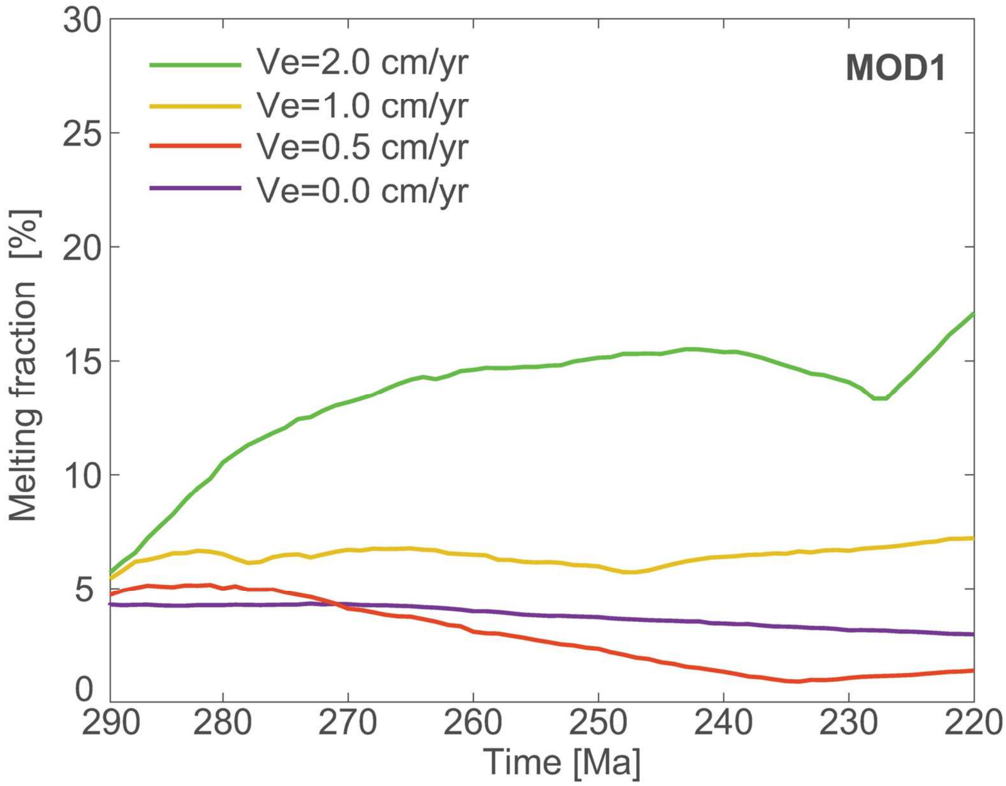

Figure 9 Melting fraction predicted from 290 to 220 Ma by MOD1 at four different extension rates. Although predictions from all configurations satisfy the thermal state for mantle partial melting, only the simulation with an extension rate of 2 cm/yr produces mantle partial melting >10%, reaching a maximum value of 15-17%.

138x108mm (300 x 300 DPI)

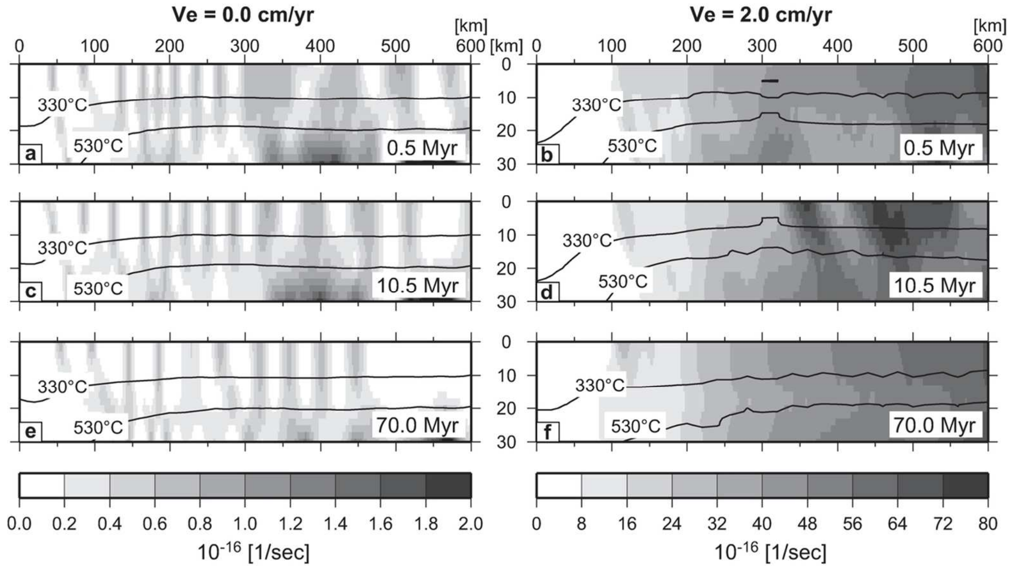

Figure 10 Variation in time (0.5, 10.5 and 70.0 Myr) of maximum strain rate at the lithospheric level predicted by model MOD1 with an extension rate of 0.0 cm/yr (a, c and e) and 2.0 cm/yr (b, d and f). Solid black lines are isotherms (330 and 530◦C). Localization of maximum shear strain in the gravitational simulation occurs at the crust-mantle interface and mainly under a compressional regime. On the contrary, in the forced extension simulations shear strain localization occurs through the entire crust and under an extensional regime. Redrawn after Marotta et al. (2009).

114x65mm (300 x 300 DPI)

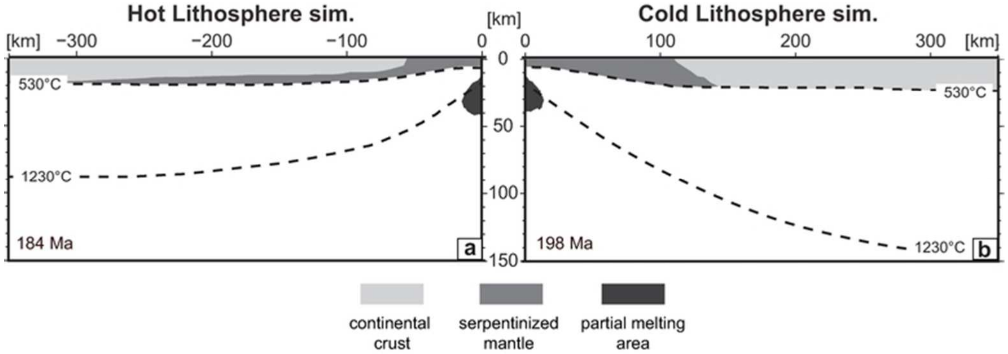

Figure 11 Thermo-mechanical setting predicted by MOD2 model for hot (a) and cold (b) lithosphere simulations at time of mantle partial melting. Dashed lines refer to 800 K (ca. 530◦C) and 1500 K (ca. 1230◦C) isotherms. In the hot configuration, the thickness of the continental crust decreases up to 5 km close to the OCTZ. In the cold model instead, the crustal thickness decreases up to approximately 20 km. Redrawn after Marotta et al. (2018).

65x23mm (300 x 300 DPI)

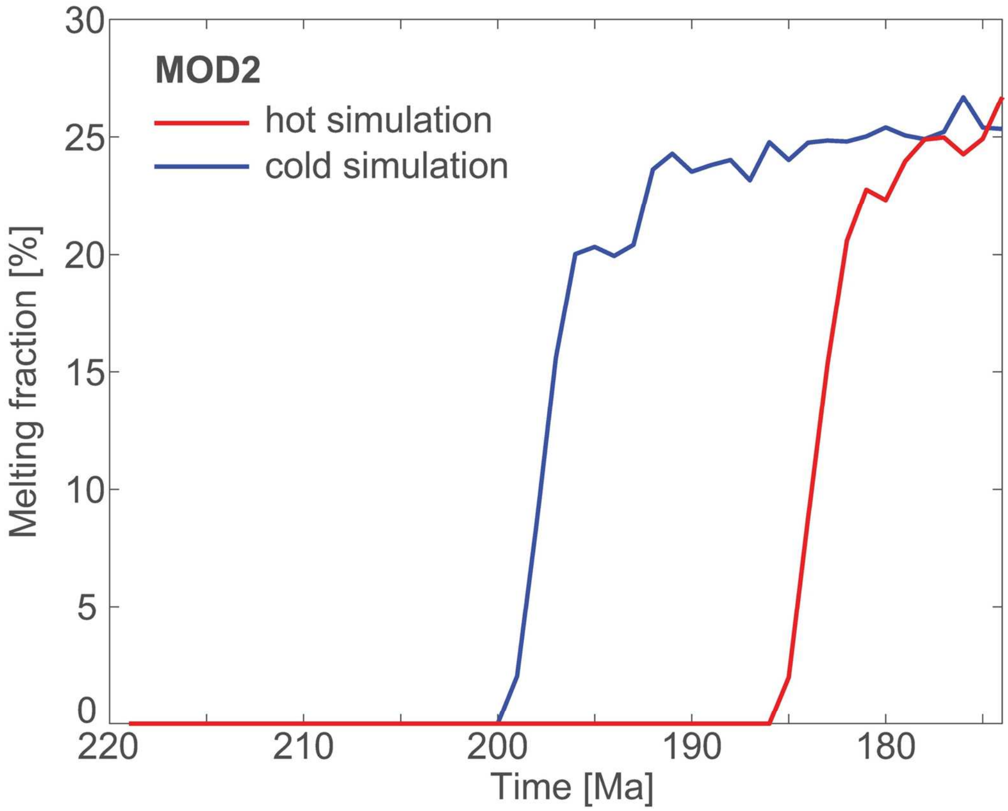

Figure 12 Predictions of melting fraction in time of the lithospheric mantle for rifting (MOD2) of two different lithosphere thicknesses and thermal states (hot and cold lithosphere). Both configurations reach a melting fraction >20%, typical for basaltic melts, but at two different time steps. For a hot and thin lithosphere it occurs after 40 Myr, while for a cold and thick lithosphere after 22 Myr.

139x112mm (300 x 300 DPI)

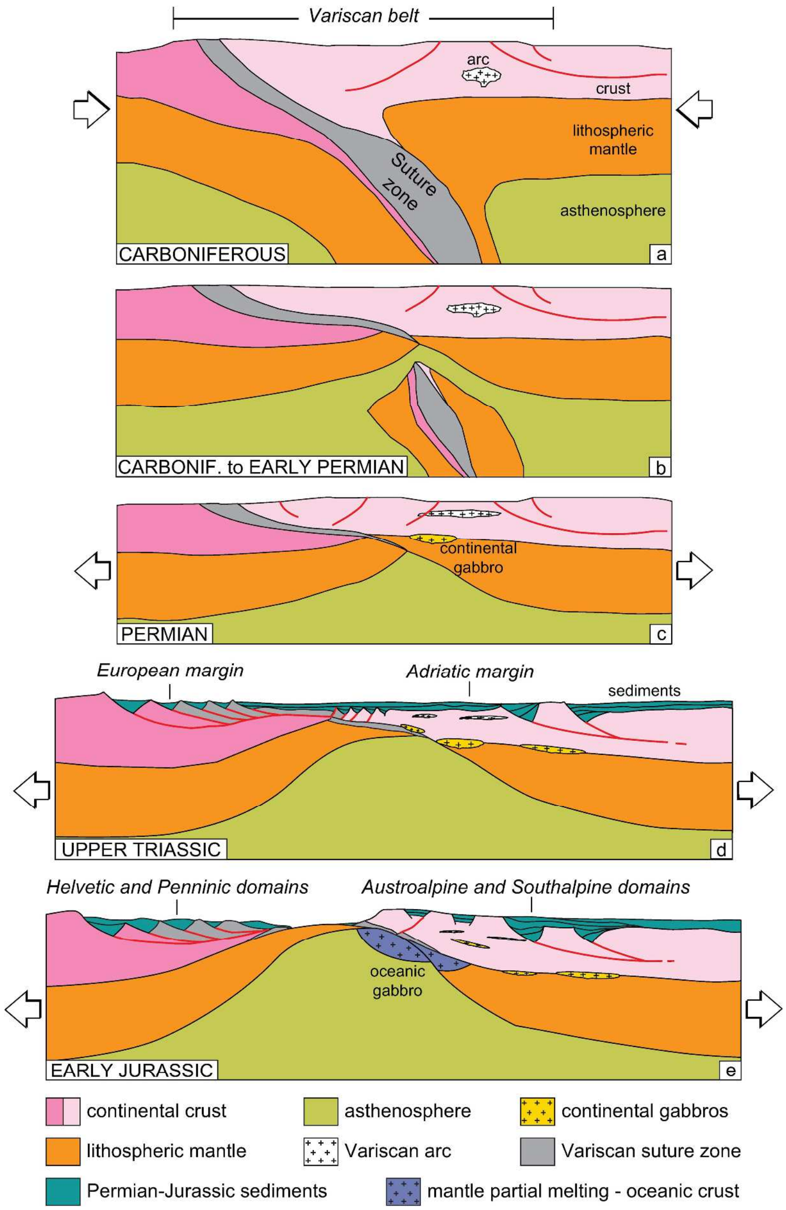

Figure 13 Geodynamic cartoon illustrating some stages of the proposed transition from late collisional slab break-off after the Variscan subduction to Jurassic ocean opening. Variscan magmatic arc after Lardeaux et al. (2014) and Delleani, Rebay, Zucali, Tiepolo & Spalla (2018). Variscan suture zone after Regorda et al. (2017). Continental crust is subdivided as belonging to the European (pale pink) or Adriatic (light pink) margin.

264x407mm (300 x 300 DPI)